Deliverable 8.1: Initial State-of-the-Art report

Work Package 8

DOI: 10.5281/zenodo.18173286

Co-funded by the European Union under Grant Agreement n°101166718

Document information

Project Acronym	**EURAD-2**
Project Title	**European Partnership on Radioactive Waste Management-2**
EC grant agreement No.	**101166718**
Work Package Title	**Release of safety relevant radionuclides from spent nuclear fuel under deep disposal conditions**
Deliverable No.	**8.1**
Deliverable Title	**Initial State-of-the-Art report**
Lead Beneficiary	**Amphos 21 Consulting**
Contractual Delivery Date	**March 2025**
Actual Delivery Date	**March 2025**
Dissemination level	**Public**
Authors	**Olga Riba (Amphos 21) and Lena Evins (SKB)**

To be cited as:

Riba O., Evins L. (2025): Initial State-of-the-Art report of deliverable D8.1 of the European Partnership EURAD-2. EC Grant agreement n°:101177718

Disclaimer

Acknowledgement

This document is a deliverable of the European Partnership on Radioactive Waste Management 2 (EURAD-2). EURAD-2 is co-funded by the European Union under Grant Agreement N° 101166718.

Status of deliverable		
	By	Date
Delivered (Lead Beneficiary)	Olga Riba (Amphos 21)	14.02.2025
Verified (WP Leader)	Lena Evins (SKB)	14.02.2025
Reviewed (Reviewers)	Michel Herm (KIT), Roberto Gaggiano (ONDRAF/NIRAS), Nieves Rodríguez-Villagra (CIEMAT), Mats Jonsson (KTH), Janne Heikinheimo (VTT)	28.02.2025
Approved (PMO)	Peter Ormai (PURAM)	13.03.2025
Submitted to EC (Coordinator)	Andra	27.03.2025

Executive Summary

The initial state-of-the-art (SOTA) report aims to compile existing knowledge and, specifically, to identify knowledge gaps that frame the objectives of the SAREC work package (WP). This document will be updated at the final stage of the EURAD-2 project, integrating key findings from SAREC WP8, relevant insights from other work packages, and recommendations for future research.

The primary goal of the research planned in SAREC WP8 is to generate data that enables a re-evaluation of current approaches to the release of safety-relevant radionuclides in post-closure safety assessments. This will help determine which existing approaches may be overly conservative and which need adjustments to better represent expected radionuclide release under deep geological repository (DGR) conditions.

The current SOTA report is structured according to the SAREC research areas and provides the foundational knowledge that underpins the experimental and modeling work undertaken in the project. Specifically, the report examines:

i) the relations between fission gas release (FGR), instant release fraction (IRF), and matrix dissolution during Spent Nuclear Fuel (SNF) leaching, ii) the radionuclide contributions from microstructural features, specifically, radionuclide release mechanisms originating from open grain boundaries, closed porosity, and rim grains, iii) the key govering processes the SNF dissolution through examining the outcome from unirradiated model materials (doped UO_2), iv) the modeling approaches—ranging in complexity and process simplification—have been developed to simulate SNF behavior over time.

By addressing these research challenges, this report lays the foundation for advancing the scientific understanding of SNF dissolution and improving the reliability of predictive models for long-term safety assessments in deep geological disposal environments. Additionally, it identifies knowledge gaps and the motivation for the current project, ensuring that SAREC research efforts are well-targeted and impactful.

Table of content

List of figures

Glossary

AGR - Advanced Gas-cooled Reactors

AP - Activation Product

ASIED - Alpha Self-Irradiation Enhanced Diffusion

BWR - Boiling Water Reactors

CANDU - Canada Deuterium Uranium reactor

DGR - Deep Geological Repository

EBSD - Electron Back Scatter Diffraction

ECW - Evolved Cement Water

EDS - Energy Dispersive Spectra

EPMA - Electron Probe Microanalyser

FGR - Fssion Gas Release

FIAP - Fraction of Inventory in the Aqueous Phase

FIB - Focused Ion Beam

FMDM - Fuel Matrix Dissolution Model

FP – Fission Product

HBS - High Burnup Structure

IRF - Instant Release Fraction

LHGR - Linear Heat Generation Rate

LWR - Light Water Reactors

MAM - Matrix alteration model

MOX - Mix of UO_2 and PuO_2 (fuel pellets)

PCI - Pellet-Cladding Interaction

PHWR - Pressurized Heavy Water Reactor

PWR - Pressurized Water Reactors

REE - Rare Earth Elements

SCC - Stress Corrosion Cracking

SEM - Scanning Electron Microscopy

SNF - Spent Nuclear Fuel

SPFT - Single Pass Flow-Through

TEM - Transmission Electron Microscope

UPC – Universitat Politècnica de Catalunya

UWO - University of Western Ontario, Canada

VVER - Water-Water Energetic Reactor

WP - Work Package

WDS - Wavelength Dispersive X-ray Spectroscopy

XAFS - X-ray Absorption Fine Structure spectroscopy

XAS - X-ray Absorption Spectroscopy

XRD - X-Ray Diffraction

1. Introduction

For a number of countries, spent nuclear fuel (SNF) is considered the ultimate waste form for geological disposal. Therefore, the physical and chemical characteristics and leaching behaviour of SNF need to be known, to help describe how radionuclide release will occur in a repository environment. The main goal of the research that has been performed in this field is to support the safety case for geological repositories and the data needs of their safety assessments. Storage and handling before final disposal must be considered as these predisposal steps may affect some important fuel characteristics. The current report is concerned with the processes involved in radionuclide release from the SNF under final disposal conditions (excluding the metallic structural materials).

1.1 Spent Nuclear Fuel – an overview

A detailed summary of the physical characteristics of nuclear fuel, and what controls radionuclide formation and distribution in SNF, is given by Spahiu (2021) in his report on the State-of-Knowledge in the Spent Nuclear Fuel Domain. In the current report, an overview is provided to serve as an introduction to the issues that are relevant to radionuclide release from SNF.

The types of nuclear fuel that are used today are mainly designed for use in Light Water Reactors (LWR), which include Boiling Water Reactors (BWR) and Pressurized Water Reactors (PWR). These fuels consist of long stacks of cylindrical UO_2 pellets inside a fuel cladding made of a corrosion resistant alloy, almost exclusively based on Zr. The pellets may also be made up of a mix of UO_2 and PuO_2, called MOX. The number of rods in each fuel assembly vary depending on reactor type. A BWR fuel assembly will normally have between 64 and 100 rods, while a PWR assembly will have between 225 and 289 rods. The rods are arranged in grids, normally in an assembly with a square cross section (Figure 1.1) There are some variations, with respect to these configurations, such as in the case of the water-water energetic reactors (VVER), a form of PWR reactors for which the fuel assembly has a hexagonal cross section. Some fuel assemblies, such as the ones for the Canada Deuterium Uranium (CANDU) reactor (a type of Pressurized Heavy Water Reactor, PHWR) and the Advanced Gas-cooled Reactors (AGR), which use UO_2 fuel and CO_2 gas as coolant, have a circular cross section. Notably the pellets in the AGR design are hollow, to allow gas circulation. In addition, there are some novel fuel types under development for research reactors or new types of reactors, such as TRISO. The majority of the current SNF inventory is however in the form of UO_2-based fuel rods, and this is what the current report is focused on.

Figure 1.1. Left: Part of a BWR nuclear fuel assembly: Svea-96 Optima3 by Westinghouse. From https://info.westinghousenuclear.com/blog/svea-96-optima3 Right: Fresh UO_2 fuel pellets. From https://www.nrc.gov/reading-rm/basic-ref/glossary/pellet-fuel.html

In LWRs the U has to be enriched in the fissile isotope U-235, or, for MOX, the fissile isotope Pu-239. A higher enrichment allows for more fission from the fuel, allowing longer use (burnup) and more energy from each fuel assembly before it is considered spent. The trend over time has been to increase the enrichment. Commonly in LWRs the enrichment is limited to ca 5% U-235. The burnup, measured in the unit MWd/kgU, has also increased to values just below 60 MWd/kgU. A fuel with burnup higher than ca 45 MWd/kgU is considered a high burnup fuel. With regards to enrichment and burnup, it should be noted here that the PHWR nuclear fuels, such as the CANDU fuels, do not use enriched U but rather natural uranium and therefore spent PHWR fuels have a much lower burnup than spent LWR fuels.

During reactor operation, radionuclides are formed via fission and neutron activation in the fuel pellets, and by neutron activation in the fuel assembly construction materials. There will normally also be some corrosion products that have deposited on the fuel rods, called crud, that also contain radionuclides. Fission produces a range of fission products. Most of the fission products formed will have atomic weights around 90 and 140 (Figure 2 in Spahiu 2021).

Some fission products are naturally volatile (*e.g.* Xe and I), while some are volatile at high temperature (*e.g.* Cs). It follows that temperature is important for the characteristics of the spent fuel. One way to estimate the temperature reached in the fuel during reactor operation is via the linear power rating, or Linear Heat Generation Rate (LHGR), measured in W/cm. Commonly for spent LWR fuels is a linear power of 15-25 kW/m, meaning ca 800°C to 1200 °C. The higher temperatures reached in a fuel rod that has experienced a high linear power rating influence the diffusion of fission products fission, in particular the fission gases (Xe, Kr) but also some volatile fission products (I, Cs). This is further discussed in section 2.1.

The operational conditions not only affect the nuclide inventory but also the fuel pellet microstructure so that the fuel pellet cracks (Figure 1.2) and swells and the fission products segregate to form aggregates of in various sizes. At high burnup the rim of the pellet recrystallizes to form a fine-grained structure called the High Burnup Structure (HBS). A good review of the HBS formation and structure is provided by Rondinella and Wiss (2010). At very high temperatures, a more pervasive recrystallization can occur, forming a central void and columnar crystals (Parrish and Aitkaliyeva 2018). However, most of the pellet normally retains the original grain size, typically ca 10 µm, and the fission products are either found inside the grains in the UO_2 lattice or as small inclusions, or along grain boundaries, or in cracks and in the gap between the pellet and cladding. At high burnup, the swelling and recrystallization at the rim of the pellet can cause Pellet-Cladding Interaction (PCI) and the gap can more or less disappear, as the Zr-based cladding bonds to the pellet (Nogita and Une 1997).

Whether the fission products segregate or not from the UO_2 matrix depends on their chemical characteristics as described by Spahiu (2021). In general, four groups of fission products are identified (Kleykamp 1985):

1. Volatile and gaseous fission products: Kr, Xe, Br, I; (Cs, Rb, Te).
2. Fission products forming metallic precipitates: Mo, Tc, Ru, Rh, Pd, Ag, Cd, In, Sn, Sb, Se, Te.
3. Fission products forming oxide precipitates: Rb, Cs, Ba, Zr, Nb, Mo, Se, Te.
4. Fission products dissolved as oxides in the UO_2 matrix: Sr, Zr, Nb, Y, La, Ce, Pr, Nd, Pm, Sm, Eu and the actinides.

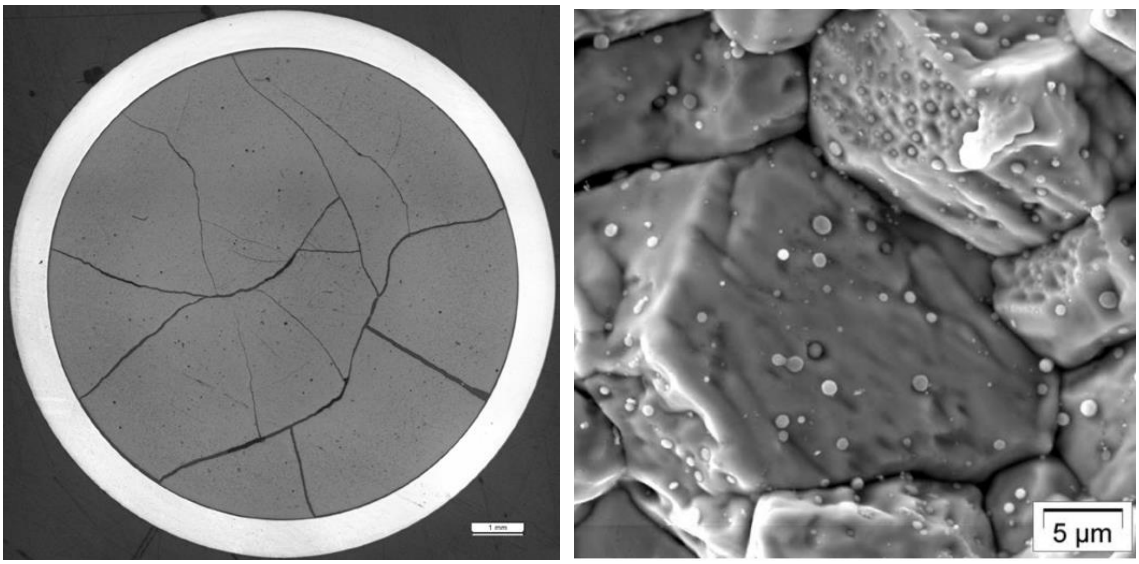

Figure 1.2. Left: Radial micrograph (Light Optical Microscopy) of a used PWR fuel with rod average burnup 43 MWd/kgU (scale bar is 1 mm). Copyright: SKB. Right: Grain surfaces in an irradiated MOX fuel. Metallic fission product precipitates are observed as round spots. From CEA (2009).

If water contacts the SNF pellet, radionuclide release will be initiated. The release rates will be different depending on where in the spent fuel structure the radionuclides are located, as well as the chemical conditions and the pellet microstructure. For safety assessments, it is important to quantify the fraction of the radionuclide inventory that will be rapidly released, and to calculate a release rate for the radionuclides located within the grains of the fuel matrix. The current report aims to summarize the state-of-the art with regards to these aspects. As mentioned above, the volatile and gaseous fission products have a strong tendency to migrate in the pellet due to the thermal gradient during reactor operation. Thus, a certain fraction of these will separate from the UO_2 matrix and be found in the cracks and gap between the pellets and the cladding. The amount of fission gases that have escaped to the gap and plenum can be measured during post-irradiation examinations by puncturing the fuel cladding and measuring the amount of gas released. This is called the Fission Gas Release (FGR), an important parameter related to the research concerning radionuclide release from SNF. This is further discussed in section 1.2.

1.2 Scope

The aim of the research planned in the EURAD-2 work package SAREC (WP8) is to provide data that allows re-evaluation of the current approaches to the study of the release of safety relevant radionuclides in post closure safety assessments. This will clarify what approaches are overly pessimistic and what approaches need to be adjusted to better represent expected radionuclide release in the repository environment. The work performed in WP8 starts off using the State of Knowledge in the Spent Nuclear Fuel domain as described by Spahiu (2021) as a stepping stone. The research is planned based on identified knowledge gaps, results and experiences of previous collaborative EU-projects, mainly the FIRST-Nuclides, DisCo and REDUPP projects (Kienzler *et al.* 2014, Evins *et al.* 2014, Evins *et al.* 2021).

1.3 Structure of the report

The aim of this report is to summarise the state of the art at the start of EURAD-2 WP8 SAREC, specifically in the areas of concern for the following objectives:

- Improving quantification and mechanistic understanding of the release of safety relevant radionuclides during leaching, covering most representative types of SNF. In particular, the relationship between FGR, Instant Release Fraction (IRF) and matrix dissolution (Chapter 2).
- To discriminate radionuclide contributions from open grain boundaries, closed porosity and rim grains during alteration, secondary phase formation during leaching/dissolution of SNF under conditions relevant for deep geological disposal (Chapter 3).
- Quantifying and understanding the mechanisms of specific processes governing matrix dissolution and those related to the release of safety relevant radionuclides during SNF dissolution, *e.g.* the effect of surface area, the fission products and noble metal particles, the pellet-cladding interaction (PCI), secondary phase formation and water radiolysis (Chapter 4).
- Improving and developing mechanistic models related to the release of safety relevant radionuclides from SNF, to include for example: i) to account for the release of matrix, grain boundary and gap (at scale of SNF pellet); ii) to integrate the effect of different amount of epsilon particles on the release of AP, FP and matrix dissolution; iii) interpretation or transposition at the DGR scale: which process(es) prevail in the different phases expected in repository conditions (e. g. Fe/H_2 effect) (Chapter 5).

2. Release of radionuclides during leaching of SNF

2.1 Instant release

Some radionuclides in the SNF structure, described in section 1, are more accessible and loosely bound and thus more easily leached than others, resulting in a rapid release when water contacts the SNF. This fraction of the radionuclide inventory is called the “Instant Release Fraction” (IRF) since the release is modelled as instantaneous in the radionuclide transport calculations. In reality, the release normally occurs over a few months up to a year (Kienzler *et al.*, 2014). This is however more or less instantaneous in the time perspective of deep geological repositories, the releases from which are analysed for many thousands of years. Therefore, the focus IRF leaching studies has historically mainly been to quantify how large this fraction is for the different radionuclides involved, rather than to try to determine the release rate and what controls it.

Spahiu (2021) provides a summary of the state of knowledge in this area of research. As described there, the IRF is defined as the fraction of radionuclides that is released faster than the spent fuel matrix. Therefore, this fraction can be located in both the gap, the grain boundaries and cracks. Generally, the following radionuclides are included in the IRF (SKB 2022):

C-14, Cl-36, Se-79, Sr-90, Tc-99, Pd-107, Sn-126, I-129, Cs-137, Cs-135

There is a consensus that the FGR, meaning the fission gases (Xe, Kr) released to the gap between the fuel pellet and the cladding and the plenum, can be used to quantify the IRF for radionuclides that are gaseous during the reactor operating temperatures (Spahiu 2021). Of the fission products, these are mainly I-129 and the Cs isotopes. For Se-79, some correlation to FGR is assumed but it less clearly understood; data from the FIRST-Nuclides project indicate that Se is mainly chemically incorporated in the SNF matrix (Curti *et al.* 2015), which can explain the experimentally determined very low fractional release of Se (Johnson *et al.* 2012). A correlation to FGR is also used for the activation product Cl-36 since it is expected to diffuse rapidly at higher temperatures. For the other radionuclides in the list, experimental leaching data are used to quantify the IRF (SKB 2022). Spahiu (2021) also discusses ASIED (Alpha Self-Irradiation Enhanced Diffusion), and the question of the pellet rim inventory; the conclusion from previous projects is that neither ASIED nor the rim inventory need to be taken into account when quantifying the IRF.

This section is focused on the IRF of I and Cs, and how well this can be determined by knowledge of the FGR. The relation between IRF, FGR, burnup and linear power rating is central to these studies. In his summary of the results from the EC-project FIRST- Nuclides, Spahiu (2021) describes how IRF of I and Cs was investigated as a function of burnup and linear power rating: at high linear power ratings, above 25 kW/m, correlation between IRF (Cs and I) and linear power rating is stronger than the correlation between IRF (Cs and I) and fuel burnup. The results from FIRST-Nuclides, summarised by Lemmens *et al.* (2017) show overall a large scatter in the data for I (Figure 2.1).

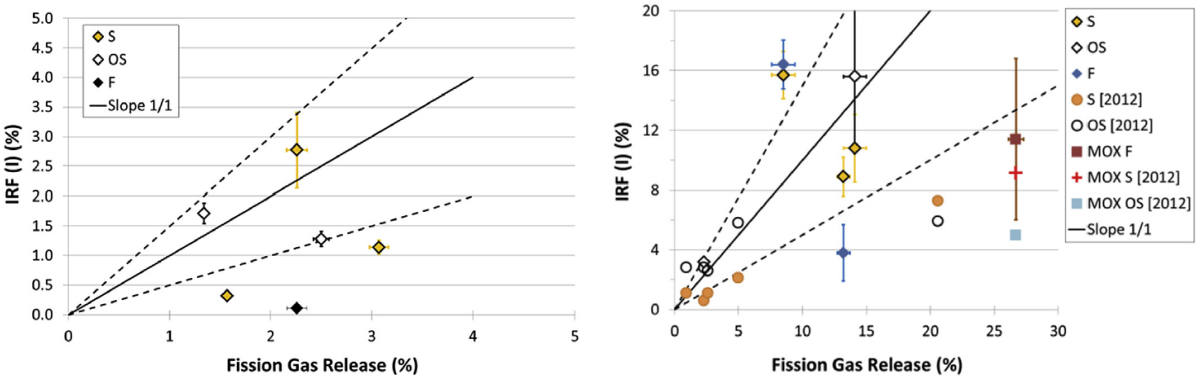

Figure 2.1. Cumulative IRF of iodine vs FGR. *(Lemmens et al. 2017). Left: BWR fuels, Right: PWR fuels including MOX. S = Segment, OS = Open Segment, F= Fragments. Dashed lines indicate IRF deviations of ±50% from the ideal slope 1/1 (solid line).*

Up to now, only a few IRF-focused studies have adjusted the leaching environment to mimic the reducing repository conditions expected. The reason for this is mainly practical: for simply quantifying the fraction of rapidly released radionuclides, there is no need to study the mechanism or rate of release. In addition, experiments in contact with air are normally more easily conducted than experiments with controlled atmosphere. Thus, most IRF studies have been carried out in presence of air (Spahiu 2021), with no attempts to analyse gaseous release during leaching. A notable difference is the experiments performed by KIT-INE (González-Robles *et al.* 2016) in the FIRST-Nuclides project, in which the IRF was studied in an autoclave with reducing gas phase (Ar + H_2), and gas release from the SNF sample was monitored. The observed surprisingly large fraction of the fission gases released during leaching (15-25%) triggered further questions. The following conclusions were made in the FIRST-Nuclides project: "*The existence of a continuous fission gas release mechanism and parallel iodine release mechanism during the leaching was demonstrated, but it is not yet clear to which extent this process is influenced by the fuel production process, fuel properties, sample preparations or leach conditions*" (Lemmens *et al.* 2017). It was however pointed out by Lemmens *et al.* (2017) that the fuel used by Gonzales-Robles *et al.* (2016) had a high FGR upon puncturing (ca 8%) and that sample preparation or fuel fabrication method (NIKUSI), might have influenced the fission product release. Fission gas release during leaching has also been shown to be high (28%) for a very high burnup fuel (Puranen et al 2022), but quite modest (indicated ~1-1.5%) for another fuel with high burnup (Puranen et al 2018), strengthening the case for further investigation of this issue.

The results from FIRST-Nuclides (Figure 2.1), and especially the study of Gonzales-Robles *et al.* (2016), triggered concerns about the simplified approach of equating the FGR, as measured when the cladding is punctured, and IRF. Other questions that arise from studying IRF under reducing conditions are related to leaching mechanisms of grain boundaries and the release of radionuclides residing there. For example, the concentrations of isotopes typical for metallic particles (Tc, Mo Ru, Rh, Pd), often found in grain boundaries, are very low during these conditions (Spahiu, 2021). This likely means that the measured released fraction is less than the fraction segregated from the UO_2 matrix, and thus illustrates

one issue arising from using the simple definition of IRF as the fraction of the radionuclides segregated from the matrix.

Another aspect of the IRF studies are the leaching conditions, in particular water composition. Some results connected to the DisCo project (Evins *et al.* 2021) that were recently published (Iglesias *et al.* 2023) show that IRF of Cs in aerated conditions differs depending on the expected repository environment. Iglesias *et al.* (2023) observed that IRF of Cs is higher in water characteristic of cement-based repository, compared to the simpler water composition used to mimic repository environments in granitic bedrock.

As mentioned above, the modelling approach in safety assessments is generally to use the known (measured and/or calculated) FGR from reactor operation, *i.e.* the gas that has been accumulated in the gap and other voids and easily accessed areas of the spent fuel rod, to determine the IRF for I and Cs. Even though many experiments show that the IRF of Cs is more the 1/3 of the FGR, the pessimistic approach is to use a 1:1 correlation for both I and Cs (*e.g.* SKB, 2022). Alternatives to this simplistic modelling approach has been suggested (see for example Espriu-Gascon *et al.*., 2020) and some efforts were made in the FIRST-Nuclides project (Kienzler *et al.* 2014) to improve our understanding of the details of radionuclide mobilisation along the grain boundaries, including the penetration of water into the fuel sample.

The SERNIM model developed by Espriu-Gascon *et al.* (2020; see section 5.1) used data from the core of a spent BWR fuel experiment (Martinez-Torrents *et al.* 2017) performed in oxidizing conditions. The rod average burnup and FGR of the fuel used is fairly standard: 42 MWd/kgU, and FGR ca 2.3%. The linear power rate is perhaps on the high side for the BWR with this burnup: 217 W/cm, and, most notable, the sample from the core is in powder form. The sample preparation can have a large influence on the radionuclide release pattern. For the “core” experiment of Martinez-Torrents *et al.* (2017), this is shown by a Cs fractional release reaching 5% after only 30 days, while the segment sample (with cladding still attached) show less than 0.3% Cs released in 190 days.

The effect of sample type was investigated by Roth *et al.* (2019) who present data indicating that using rod segments, with cladding still attached, could cause variable release over time depending on water access into the gap. As leaching progresses, new pathways can open up and cause sudden leaps in I and Cs release. Roth *et al.* (2019) also note that when the fuel sample is milled to a powder, not only the grain boundaries but also the interior of the grains are exposed, thus yielding data representing a mix of IRF and fuel matrix leaching. A similar observation was made by Barreiro Fidalgo *et al.* (2021), albeit the fine fragmentation of the fuel was not intended, but related to the sample chosen, sample preparation and, potentially, fuel type; see discussion in section 3.

2.2 Matrix release

The main fraction of the radionuclide inventory resides in the SNF matrix. The rate with which this fraction will be released, once water has contacted the fuel in the repository, is central to most safety assessments. Spahiu (2021) describes the current knowledge concerning matrix dissolution in the presence of air as well as in repository-like conditions. The most important aspect of the SNF matrix dissolution is the U redox sensitivity, and the much higher solubility of U(VI) compared to U(IV). As radiolysis produces oxidants the oxidation of U can happen even in anoxic environments (*e.g.* experiments with Ar in the gas phase). This is further discussed in section 2.2.1. If H_2(g) is present, in a closed environment, experiments show that the oxidation of U is efficiently inhibited (Spahiu 2021), see section 2.2.2. Additional questions concerning how fuel characteristics may affect the matrix dissolution are discussed in section 2.2.3

2.2.1 Radiolysis and oxidation

As described by Spahiu (2021), the radiation from spent fuel is complex, consisting of α, β, and γ radiation. This means water surrounding the fuel will be affected by radiolysis, and produce very reactive radicals ($OH^{\cdot}$, $H^{\cdot}$, $OOH^{\cdot}$, e_{aq}^{-}) and molecules (H_2O_2, H_2, O_2). The low reactivity of H_2 leads to oxidizing conditions at and near the fuel surface. Since radiolysis of water has been well studied over the years, this will not be described in detail here. The reader is referred to Spahiu (2021) and references therein. It will suffice to say that for repository conditions, it is mainly the alpha radiolysis at the spent fuel surface that will be of importance. The oxidants produced near the surface oxidize UO_2 and thus changes the solubility of U which is then released into solution.

SNF leaching studies have been performed since the 1970s. At that time, the leaching studies were mainly performed in contact with air. A description of these studies is given by Spahiu (2021). To summarize, the studies showed 1) the clear oxidation of U due to the oxidizing conditions in the experiment 2) difficulties determine the specific surface area of SNF 3) SNFdissolution rates were estimated using Fraction of Inventory in the Aqueous Phase (FIAP) for radionuclides contained in the fuel. This FIAP parameter is most valuable for radionuclides that do not reach the solubility limit with regards to a solid phase in the experiments. For U, in some of the longer running air-saturated experiments, the solubility limit for some U(VI) phases were reached and therefore, the U concentration is reported rather than FIAP. The FIAP of Sr was used to estimate a fractional rate of ~10^{-7} d^{-1} under oxidizing conditions (Forsyth 1997, Grambow *et al.* 2000). The results of Forsyth (1997) are given in Figure 2.2. This translates to ~10^{-5} yr^{-1}.

The processes involved in the oxidative dissolution of spent fuel have been studied for as long as spent fuel experiments have been performed, since it is at the core of understanding what controls the spent fuel dissolution rate. SNF is a complex material that contains a multitude of elements; to better understand the oxidative dissolution of UO_2 matrix, simpler experimental systems were set up. These experiments involved either pure UO_2, or UO_2 with various additives; the most complex material being SIMFUEL containing 11 oxides mimicking fission products (Lucuta *et al.*. 1991). To study the effects of radiation, either the experiments were irradiated with a gamma source, or the material itself was doped with alpha-emitting isotopes. For alpha radiolysis, it was shown in the 1980s, based on results from electrochemical experiments, that the main oxidant responsible for U oxidation is H_2O_2 (Spahiu 2021). Later experiments and simulations have also supported this conclusion (Ekeroth *et al.* 2006). Therefore, experiments are also conducted to investigate directly the effects of H_2O_2 on the UO_2 matrix.

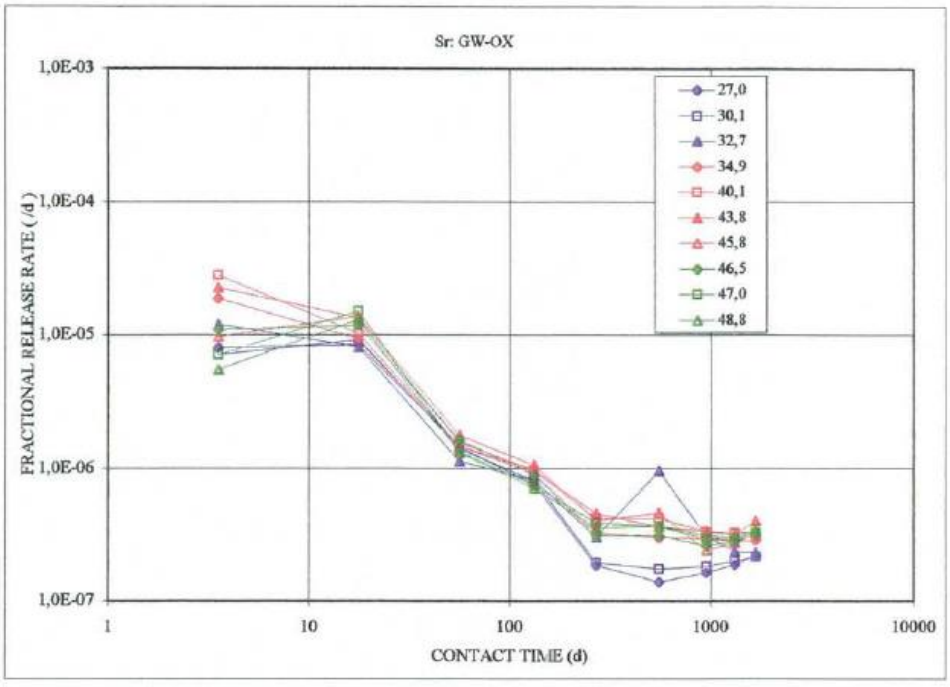

Figure 2.2. Fractional release rates based on Sr release in oxidizing conditions from SNF of various burnups. GW-OX: Groundwater-Oxidizing conditions. From Forsyth (1997).

Spahiu (2021) describes various experiments performed to provide parameters that can be used for modelling, for example, rate constants for the reactions involved. One main issue in this area is to find (or determine) rate constants that are valid for a heterogeneous system, *i.e.* for reactions that involve the interface between a solid and a liquid. A number of experiments by Jonsson and co-authors, performed to investigate the kinetics of the various reaction involved in the oxidative dissolution of UO_2 are described by Spahiu (2021). The main processes concern the reactivity of H_2O_2 towards the UO_2 surface and the two main reaction pathways: either the H_2O_2 directly oxidizes U, or the H_2O_2 is catalytically decomposed. A suggested mechanism involves surface bound hydroxyl radicals and surface sites on UO_2 (Barreiro Fidalgo *et al.* 2018), as is described in reactions 1-4.

$$H_2O_2 + UO_2 - site \rightarrow 2OH\cdot_{(ads)} \quad (1)$$

$$OH\cdot_{(ads)} \rightarrow OH^- + U(V)O_2 \quad (2)$$

$$H_2O_2 + OH\cdot_{(ads)} \rightarrow HO_2 + H_2O + UO_2 - site \quad (3)$$

$$HO_2 + HO_2 \rightarrow H_2O_2 + O_2 \quad (4)$$

This mechanism, involving surface-sites on UO_2, can help explain the lower surface reactivity at high initial [H_2O_2] as observed by Barreiro Fidalgo *et al.* (2018). In the absence of radical scavengers, the hydroxyl radical can be expected to oxidize U.

Other results relevant to heterogeneous reactions are described by Jonsson (2023), who lists reactions and rate constants that can be used for modelling radiation induced dissolution of SNF (see section 5). These include the reactions catalysed by metallic particles, such as oxidation of UO_2 by H_2O_2 and O_2, catalytic decomposition of H_2O_2, recombination of H_2O_2 and H_2 to form water, as well as reduction of UO_2^{2+} (aq) and $U(VI)O_{2(surf)}$ by H_2. Other reactions, not requiring the metallic particles for catalysis, are oxidation of UO_2 by O_2, the oxidation of UO_2 by the carbonate radical, and, finally, the dissolution of $U(VI)O_2$ by means of bicarbonate complexation. It is the last reaction that releases U into solution and giving the [U] measured in experiments. As mentioned above, if the rate of increase of [U] is used to indicate matrix dissolution, the experiment needs to be set-up so that the solubility limit of secondary U(VI)-phases are avoided.

2.2.2 Repository environments

In spite of the anoxic environment expected in most deep geological repository environments, the radiolysis, as we have seen in section 2.2.1, will still potentially cause oxidation of the U in the SNF matrix. However, all repository concepts involve a large reservoir of metallic Fe, either as cast iron or steel. As described by Spahiu (2021), this will provide both dissolved Fe and molecular hydrogen (H_2). It has been recognized for many years that this may provide a means for keeping the environment reducing, even near the SNF surface. There is also plenty of experimental evidence that anoxically corroding Fe and H_2 in the gas phase, in autoclave leaching experiments, can suppress the oxidative dissolution of U in SNF (see list of references in Spahiu 2021). Regarding the relative importance of Fe and H_2, Puranen *et al.* (2020) provides evidence for a much stronger effect of H_2 compared to Fe(aq).

In these experiments, [U] is close to the solubility limit of UO_2 (am) (log [U] = -(8.5 ± 1.0). Neck and Kim 2001) indicate that H_2 suppresses oxidative dissolution of U. In presence of H_2, there is no need for Fe in the experiment for this effect (Ekeroth *et al.* 2020, Puranen *et al.* 2018, 2022). Some recent results indicate that sample history, in particular previous exposure to oxygenated environments, can affect the

radionuclide release and cause slightly elevated [U]. However, also in cases with problematic pre-oxidation of samples, the release rate is very close to zero after one year of leaching with hydrogen in the gas phase (Figure 2.3, Barreiro *et al.* 2021), indicating no further oxidative dissolution of U.

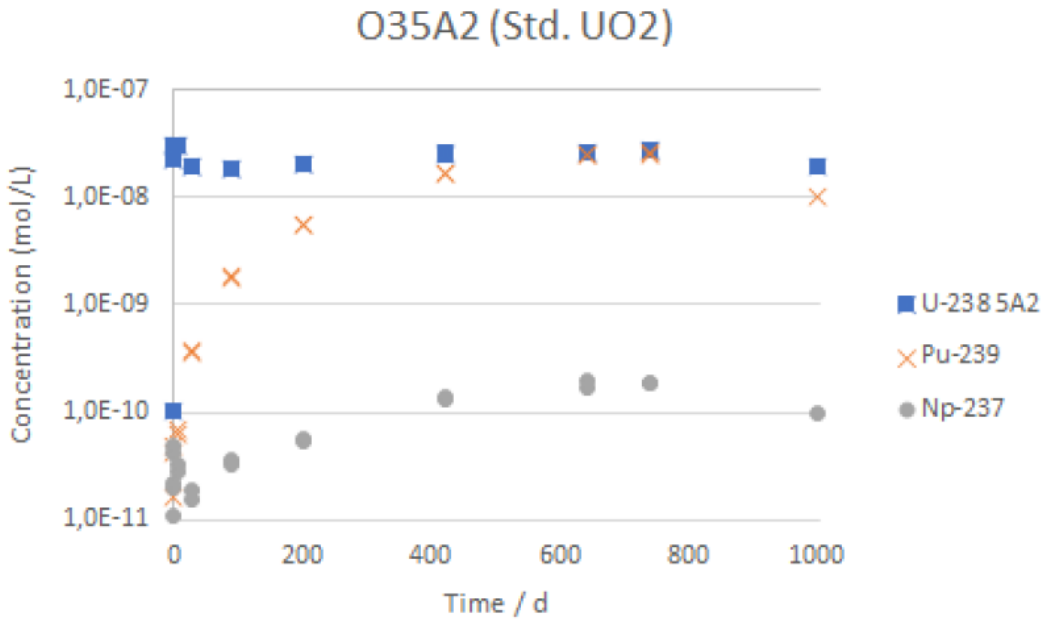

Figure 2.3. Results from leaching standard UOX fuel with H_2 overpressure. From Barreiro Fidalgo et al. (2021). The [U] is stabilized at higher levels than expected due to pre-oxidation and colloid formation.

All results from the SNF leaching experiments performed in the DisCo project are collected and discussed by Metz (2021). One observation is that during the first year of leaching, the redox conditions affect the release of actinides much more than the release of non-redox sensitive fission products, such as Cs. The measured U concentrations (Figure 2.4) show clearly the effect of redox conditions in the leaching vessel; under air and Ar atmospheres relatively rapid increase of U concentrations due to oxidation can be observed, compared with U concentrations in experiments with hydrogen overpressure. The Cs release (not depicted) cannot be used as a measure of matrix release, since it is part of the IRF (see section 2.2.1) and, in extension is closer connected to fuel characteristics (section 2.2.3) and sample history than to redox conditions.

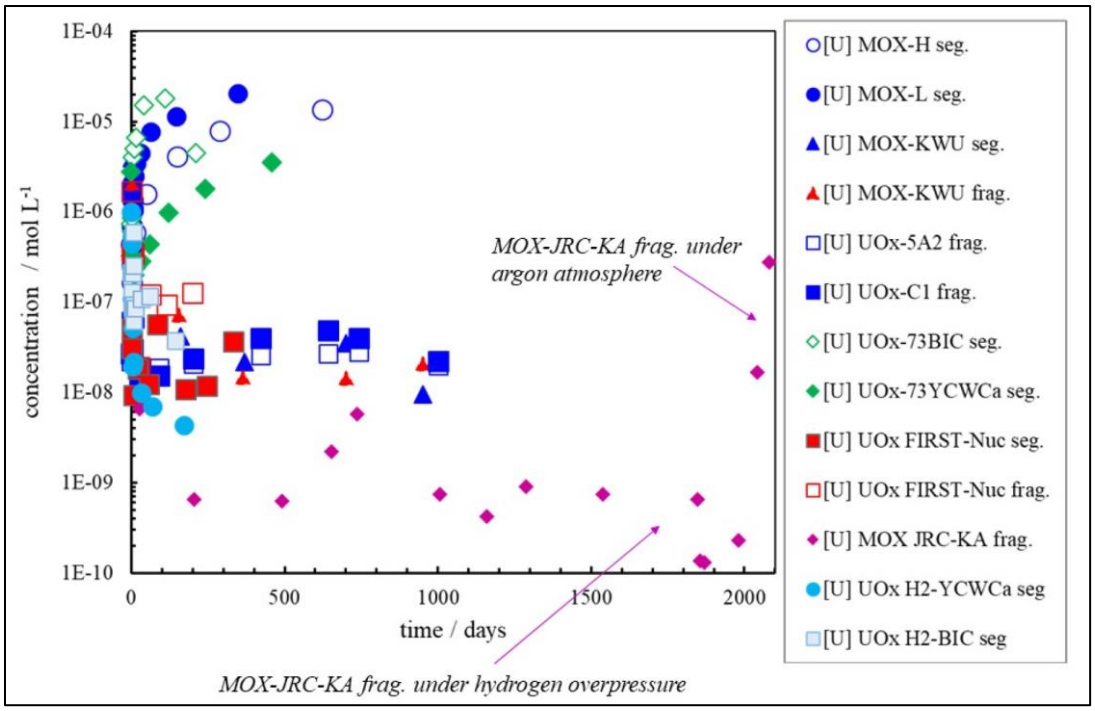

Figure 2.4. U concentrations vs. time from SNF leaching experiments performed within the DisCo project plotted together. From Metz (2021). Data are from experiments with air, Ar and H_2 in the gas phase.

The results from experiments where SNF is leached in the presence of metallic Fe provides evidence that there is negligible U(VI) in solution under these conditions (Spahiu 2021). The main argument for this is that no, or very little, U was found on the Fe surfaces. With hydrogen overpressure, it therefore seems the fuel surface is kept reduced, meaning the oxidative dissolution rate is close to zero. It follows that determining the rate of radionuclide release from these experiments is difficult; the FIAP of [U] cannot be used since it is close to the solubility limit of U(IV) solid phases, and using the FIAP of different radionuclides involves assumptions regarding the fraction of these radionuclides that are in some way segregated from the matrix (*i.e.*, the IRF, see section 2.1). One radionuclide that has been used for this purpose is Sr-90 (Grambow *et al.* 2000), since the IRF is normally very low. Even so, it is known that Sr may segregate to the so-called grey phase (Kleykamp *et al.* 1985), and this triggers further questions. However, in cases where no more Cs is released, one can argue that no more matrix is dissolved - any matrix dissolution would invariably cause a release of Cs, which is not expected to precipitate or sorb strongly in these experiments.

The discussion of the results presented above relates mostly to repository environments without cement. Cementitious materials in the repository concept are expected to strongly affect the chemical conditions. The main parameter that will be affected is the pH of the water interacting with the SNF, but also the chemical composition of the water interacting with the SNF will be affected. Therefore, a number of experiments have focused on the effects of degrading cement, using water types mimicking various stages in cement degradation, for example Evolved Cement Water (ECW), or Young Cement Water with Ca (YCWCa) (Loida *et al.* 2012). Loida *et al.* (2012) studied SNF dissolution using these waters and hydrogen overpressure and they found low matrix dissolution rates (~10^{-8}/day) and very low [U] in both experiments. Notably, in these experiments, Sr is affected by precipitation reactions and the Sr release cannot be used to estimate the matrix dissolution rate. The concentrations of Cs and fission gases did, however, reach a plateau, which means a dissolution rate close to zero. More recent experiments with cement waters and high pH were performed both in contact with air (Iglesias *et al.* 2023) and in anoxic and reducing conditions (Mennecart *et al.* 2024). The complex water chemistry may cause precipitation issues, such as calcium uranate CaU_2O_7, in oxidizing conditions (Iglesias *et al.*

2023). Hydrogen in the gas phase appear to keep U reduced also in YCWCa conditions, while [Sr], as opposed to [Cs] and [I], was lower in YCWCa compared to simpler bicarbonate conditions at near-neutral pH (Mennecart *et al.* 2024).

2.2.3 Fuel characteristics

The effect of burnup on the fuel chemistry and microstructure is discussed in detail by Spahiu (2021); in short, the higher the burnup, the more fission products and more developed High-Burnup Structure (HBS) at the rim of the fuel pellet. The connection between burnup and IRF is discussed in section 2.1 and will not be further considered here. Instead, the focus here is how burnup affects matrix dissolution and release of radionuclides from the matrix. The two main aspects of high burnup that may affect the matrix dissolution are a more fine-grained microstructure and higher radionuclide content. However, existing data show that there is no enhanced matrix dissolution from high burnup fuel. The conclusion of Spahiu (2021) is "*the high doping level at the pellet rim both with actinides (such as Pu) and fission products makes the fuel matrix less prone to oxidation and counteracts successfully both the higher surface area and the higher radiation field*." Experiments performed in contact with air and variable burnup show that in spite of higher radionuclide content at high burnup, the radionuclide release is not increased (Zwicky *et al.* 2011). Matrix dissolution for fuel with high (~65 MWd/kgU) and very high burnup (~75 MWd/kgU) has also been tested in experiments with hydrogen overpressure (Puranen *et al.* 2018; 2022), with results showing that the hydrogen successfully also supresses the fuel oxidation even for very high burnup fuels. Therefore, as Spahiu (2021) also concludes, this shows that "*fuel dissolution rates determined with average burnup fuel are valid also for high burnup fuel.*"

Even if experiments show that SNFs with various burnups yield similar results in the experimental conditions investigated, there is a need to understand the process and how the different elements in the matrix affects the redox reactivity of the UO_2. An improved understanding is required for the development of a mechanistic model in which different fuel compositions can be tested. This is why a number of studies have been performed with UO_2 pellets doped with various elements, for example Gd (Barreiro Fidalgo and Jonsson 2019), Y (+/-Pd), (Pehrman *et al.*. 2012), or Cr (+/- Al) (Rodríguez Villagra *et al.* 2022; Smith *et al.* 2023; Milena Pérez *et al.,* 2025).

The general observation is that the doped UO_2 systems exhibit a lower redox reactivity, in line with the previous preliminary evidence from electrochemical studies, where rare-earth doping was shown to suppress corrosion of UO_2 (Pehrman *et al.*. 2012, Liu *et al.*. 2017). These kinds of observations triggered a recent study on the thermodynamics of Ln-doped UO_2, in which the authors conclude that the explanation for the enhanced resistivity to oxidation is connected to a partitioning of Ln between a fluorite-type phase and a U_3O_8 polymorph (Vinograd *et al.* 2023).

In the text above, effects of burnup and dopants on the matrix dissolution and redox reactivity have been discussed. In addition, other issues concerning particular fuel characteristics are pre- and post-operational microstructure of different fuel types. Different fabrication processes can produce pellets with varying initial porosity and grain size, *e.g.* the NIKUSI process as discussed by Lemmens *et al.* (2017)**.** These aspects potentially affect the IRF more than the matrix dissolution (see section 2.1), but it is important to keep in mind that the microstructure can vary between fuel types. This is likely also one potential cause for any differences seen in studies related to Cr+Al-doped fuel (Arborelius *et al.* 2006) and Cr-doped fuel (Cardinaels *et al.* 2010); at levels of Cr-doping higher than the solubility of Cr in UO_2, Cr is found in grain boundaries (Smith *et al.* 2022), the potential effects of which on IRF are discussed in section 3. The question remains if there is a different effect of only Cr versus Cr+Al, since there is a lack of published leaching data for Cr-doped fuel under H_2 overpressure.

With regards to microstructure, there are interesting observations from different types of MOX fuels. In MOX, the Pu is either homogeneously or heterogeneously distributed in the UO_2 matrix, depending on the fabrication method. In case of heterogeneous MOX fuel, e.g. the MIMAS (MIcronised MASter blend)

MOX, Pu-rich islands in the UO_2 matrix with very high burnup occur with increasing burnup of the fuel Spahiu (2021). The effect of this on the matrix dissolution has been discussed by Jegou *et al.* (2010) and Odorowski *et al.* (2016).

3. Characterisation of grain boundaries and microstructures and their effects on leaching studies

The importance of grain boundaries and what role they play in radionuclide release during SNF leaching have been discussed for some time (*e.g.* Olander and Uffelen 2001). The argument for including a grain boundary inventory in the IRF is clearly the observation that some radionuclides do segregate and form separate phases that are to a certain degree located in the grain boundaries, *e.g.* metallic particles. However, it is well known that in general, grain boundary diffusion is faster than diffusion inside the grains (Parras and De Souza 2020), so if a radionuclide diffusing inside the grain reaches the grain boundary, it will diffuse more rapidly along the grain boundary to the gap.

Studies specifically investigating the grain boundary inventory are presented in section 3.1. Related studies, but focused more on microstructures and mechanisms involved in the preferential leaching of grain boundaries are presented and discussed in section 3.2

3.1 Grain boundary radionuclide inventory

The fraction of the fission product inventory that is located in the grain boundaries can be theoretically estimated, via models taking the temperature and diffusion coefficients into account (*e.g.* Speight and Turnbull 1977), or by experimental observation (*e.g.* Thomas *et al.* 1992).

An overview of the processes behind segregation of a fraction of the inventory to the gap and grain boundaries is given by Spahiu (2021), who focuses on how soluble the fission products are in UO_2. In general, the migration of radionuclides from the centre to the rim of the pellet is driven by the steep radial temperature gradient from the hot centre to the fuel surface. Some radionuclides have a tendency to precipitate in secondary phases, such as metallic particles, or “grey phases“ (Kleykamp et al 1985). The nucleation of these secondary phases in the grain boundaries will increase the grain boundary inventory The grain boundaries may also host inter-granular fission gas bubbles. Spahiu (2021) notes that these grey phases, more specifically perovskite-type oxides of the form $BaZrO_3$, are observed in fuel that have experienced very high temperatures. A perovskite phase is also observed on grain boundaries in SIMFUEL (Lucuta *et al.* 1991). Apart from Ba and Zr, the grey phases may contain a fraction of the Sr, Cs and Mo inventory of the fuel, so that the structural formula is more accurately described as $(Cs,Ba,Sr)(U,Mo,Zr)O_3$. The partitioning of fission products into the grey phase have been investigated since this may cause volume changes such as swelling or contraction of the fuel (Cooper *et al.* 2014).

Theoretical studies concerning how fission products segregate and remain as separate phases in the grain boundaries of UO_2 are based on thermodynamics and diffusive properties of the solid and the radioelements. Atomistic simulations focused on the properties of grain boundaries in UO_2 indicate that the impact of the formation of amorphous grain boundaries can be significant with regards to *e.g.* fission product behaviour, and formation. Further work is required in this area (Middleburgh *et al.*. 2021). Very few studies have experimentally investigated the grain boundaries of SNF. The ones that have been published note a general lack of grain boundary segregation, as seen with Transmission Electron Microscopy (Thomas *et al.* 1992) or a Cs accumulation in some grain boundaries, as seen with Electron Microprobe analyses (Mennecart *et al.* 2014). This illustrates the difficulty in verifying the predictions of the models and theories concerning the migration of IRF radionuclides such as Cs to the grain boundaries.

The metallic particles, containing Mo, Ru, Tc, Rh, Pd, are briefly described by Spahiu (2021), and a more detailed summary is provided by Spahiu and Evins (2013). The metallic particles can be very small (nm-sized) up to micrometre-sized. They are found both within grains and in grain boundaries (see Figure 3.1); in general, larger particles are often located in grain boundaries (Thomas *et al.* 1992). The fraction of these metals that have migrated to the grain boundary before precipitating, and the size of the particles, depends in part on the fuel operation, and specifically fuel temperature. In the central part of the fuel pellet the metallic particles are larger, while they are much smaller at the rim of the pellet. For normally operated LWR fuels, with pellet centre temperatures rarely above 1200 ºC, the metallic particles are usually less than 1 µm in diameter (Spahiu and Evins 2013).

With regards to the fission gases, they may collect in grain boundaries as inter-granular bubbles. When these bubbles grow, they may coalesce and create pathways to the gap and thereby escape to the plenum. There are suggestions that the mechanism for fission gas release differs depending on the temperature of operation and level of burnup (Willett *et al.* 2020). The importance of inter-linked tunnels appears to be connected to high burnup fuels, while at intermediate and low burnup, bubble diffusion and classical diffusion of single gas atoms may be the main release mechanisms (Willett *et al.* 2020). Thomas *et al.* (1992) observed nanometer-sized gas bubbles along the grain boundaries within the rim regions of the examined fuels. Further explanation on the bubble formation mechanism is included in section 5.2.

Considering the importance of grain boundaries with regards to their potential to store radionuclides and thereby affecting the way their release can be expected to happen in the repository, the effect of fuel grain size needs to be investigated. However, the recrystallization of the fuel during high burnup, for example the development of the High Burnup Structure at the pellet rim, has been shown not to increase the IRF (Spahiu 2021 and references therein). This indicates the importance not only to better quantify the grain boundary inventory, but also how accessible the grain boundaries are to the leaching solution. This is discussed below (section 3.2).

3.2 Preferential grain boundary leaching

The simple approach in safety assessments is to define the IRF as the fraction of the fuel radionuclide inventory that is released faster than the rate of the fuel matrix (Spahiu 2021). For the grain boundaries to contribute to the IRF, they need to be accessible to the leaching solution and provide a pathway for the segregated radionuclides to bulk solution. The wetting of fuel was studied via modelling in FIRST-Nuclides (Kienzler *et al.* 2014); the conclusion was that the wetting is very fast on a repository timescale, meaning there is nothing to gain by incorporating the time for wetting in the safety assessment model. Also, the many grain boundaries in the fine-grained structure of the high-burnup rim were suggested to cause a higher fraction of rapidly released radionuclides. This was however shown not to happen, meaning the grain boundaries of the rim was not preferentially leached. Concerning grain boundaries in general, Johnson *et al.* (2012) concludes: "*The data obtained here do not support the hypothesis that the radionuclides segregated at grain boundaries are easily leached. Methods of differentiating between release from the gap and from grain boundaries should be further explored.*"

How to separate the release from gap and grain boundaries is not trivial; some spent fuel experiments have tried to specifically leach grain boundaries. The experiments of Gray *et al.* (1991) introduced the method of first leaching the sample, to ideally remove the gap inventory, and then crushing the fuel sample to a grain sized powder which was then leached. The resulting grain boundary inventory was found to be generally less than the gap inventories and relatively low (1% or less). A similar approach was attempted for a SNF with very high burnup (ca 75 MWd/kgU), but with questionable results due to oxidation and exposure of inter-granular surfaces (Puranen *et al.* 2016, Roth *et al.* 2019). It seems trying to mill a SNF in order to only expose the grain boundaries for leaching is difficult.

Studies on grain boundaries were performed in the REDUPP project (Evins *et al.* 2014). Using Atomic Force Microscopy and Electron Back Scatter Diffraction techniques, Corkhill *et al.* (2014) studied CeO_2 and ThO_2 and observed preferential leaching of grain boundaries resulting in enhanced dissolution rates. They also noticed that grain boundaries with high misorientation angle retreated more rapidly than that with low misorientation (Figure 3.1).

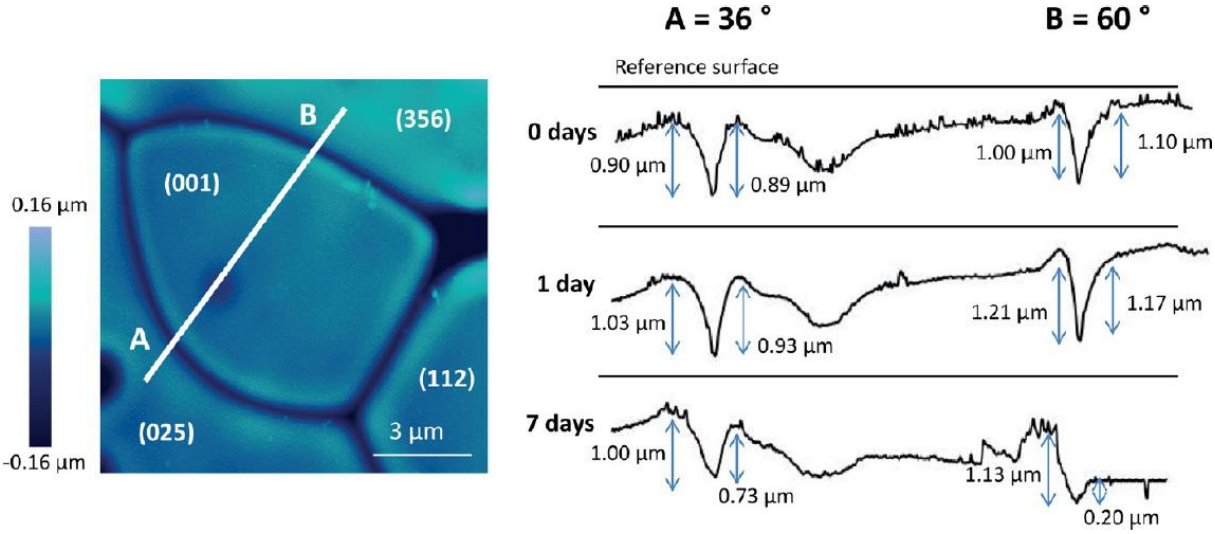

Figure 3.1. Evolution of CeO2 grain boundaries during dissolution. A: low misorientation. B: High misorientation. From Corkhill et al. (2014).

Enhanced dissolution rates are also observed in studies on UO_2 grain boundaries (Römer *et al.* 2003). Using AFM, dissolution was shown to result in typical V-shaped grain boundaries, indicating preferential leaching from these sites, potentially due to enhanced oxide conductivity to non-stoichiometry in the grain boundaries (Römer *et al.* 2003).

Defining the IRF as the gap and the grain boundary inventories combined has been a continuous source of questions and discussion, prompting attempts to refine the model. There have been attempts to extract a specific release rate from grain boundaries based on radionuclide release data (*e.g.* Johnson *et al.* 1985, Espriu-Gascon *et al.* 2020). However, as Kienzler *et al.* (2017) points out, none of the Cs and I data from the FIRST-Nuclides project follows the curves suggested by Johnson *et al.* (1985). The SERNIM model (Espriu-Gascon *et al.* 2020) is discussed in section 2.1 and section 5.1; it is noted here it is based on data from leaching of powder, and as discussed above, powder leaching may introduce some complications confounding the data interpretation.

3.3 Methods for solid and grain boundary characterization

To study how grain boundaries may influence the leaching results, the solid samples need to be characterized well, preferably before and after leaching. Methods involved in this are, as exemplified above, AFM and EBSD, but in addition the following methods, listed by Evins *et al.* (2021) can be used:

- Archimedean density method.
- He pycnometry for density determination.
- BET (Brunauer–Emmett–Teller) for surface area measurements.
- Optical microscopy for microstructural analyses.
- SEM (Scanning Electron Microscopy) with EDS (Energy Dispersive Spectra) and EBSD (Electron Back Scatter Diffraction).
- EPMA (Electron Probe Microanalyser) with WDS (Wavelength Dispersive X-ray Spectroscopy)

- XRD (X-Ray Diffraction).
- Raman spectroscopy.
- XAFS (X-ray Absorption Fine Structure spectroscopy).

Another useful tool, especially interesting for the study of grain boundaries, is Focused Ion Beam (FIB) by which the sample can be milled in order to expose new surfaces for study. Thin lamella can be produced to further study in a Transmission Electron Microscope (TEM) or X-ray Absorption Spectroscopy (XAS). One example is the work of Curti *et al.* (2015) in which, a FIB lamella from SNF was transported internationally for further study by micro-XAS. Using FIB in combination with appropriate methods can reveal insight into both the grain boundary inventory and how the grain boundary microstructure and crystallography may influence the leaching and radionuclide release.

4. Dissolution studies of model materials

The single and multiparametric studies of model materials allow the determination and quantification of the key processes driving the SNF dissolution, under geological repository conditions, associated with the presence of dopants, the grain size, microstructure characteristics, surface area, radiolysis, etc. Moreover, working with unirradiated material avoid the complexity associated with handling high doses and the complexity in results interpretation. The UO_2-based model materials are systematically prepared and precisely characterised with the aim to understand several single and linked effects on SNF dissolution under relevant storage conditions. Something to highlight is that the specific synthesis conditions of doped samples, including the cooling step, affects the final crystalline structure and redox state of dopants and, consequently, this information should be provided, specially, if an inter-comparison exercise between experimental data is intended. In this regard, the development of a common leaching protocol, including solid sample characterization and leachate analyses should be also harmonized.

4.1 Alpha doped UO_2

In Spahiu (2021) a section is dedicated to discussing the leaching behaviour of alpha doped UO_2 under anoxic and reducing conditions emphasising the effect of the increasing alpha activity on the fuel oxidation process. The leaching of UO_2 doped with wt% of alpha emitters: ^{233}U or ^{238}Pu, under anoxic conditions (Ar flushing) and carbonate solution, indicates that below the α-activity range between 3.3 and 33 MBq/gUO_2, significant dissolution attributed to alpha-radiolysis cannot be observed under this conditions (Rondinella *et al*. 2004 and Muzeau *et al*. 2009; Carbol *et al*. 2005). At pH_2 of 1bar and in carbonate solution, significant dissolution is observed above 385 MBq/gUO_2 (Muzeau *et al*. 2009). In the framework of DisCo EU-project, the effect of H_2 in alpha doped UO_2, with ~18 MBq/gUO_2, was also tested using 10bar of H_2 and Pd/Pt catalyst. Under these conditions, the U concentration was significantly greater than the UO_2(am) solubility, with final concentration of 10^{-7} and $5{\cdot}10^{-7}$ M, in both carbonate solution and young cement water. These results indicate that dissolved H_2 was unable to prevent the short-term radiolytically oxidation/dissolution process, or to reduce oxidised U(VI) in solution (Cachoir *et al.* 2021). In the light of these results and as pointed out in the DisCo final report (Evins *et al.*. 2021), the alpha activity from which significant UO_2 oxidative dissolution process is identified, remains an uncertainty under conditions of H_2 pressure.

The presence of Pu in an unirradiated homogeneous mixed oxide fuel $U_{0.73}Pu_{0.27}O_2$, with an alpha activity of 2200 MBq/gUO_2, under anoxic conditions (carbonate water under argon) limits the oxidative dissolution process due to radiolysis compared with an undoped UO_2 (Kerleguer *et al.*. 2020). The long-term dissolution rate $U_{0.73}Pu_{0.27}O_2$ was $7.6{\cdot}10^{-6}$ mol·m^{-2}·d^{-1} with H_2O_2 below the detection limit of 10^{-7} M and constant Pu concentration at 10^{-9} M, corresponding to solubility limit by $Pu(OH)_4$ (am) phase. The low concentration of H_2O_2 is attributed to a higher catalytic disproportionation of H_2O_2 on the Pu-enriched layer estimated as 99%, against 86% calculated for UO_2 (Kerleguer *et al.*. 2020).

The effect of metallic Fe on the leaching behaviour of α-doped UO_2 appears much clearer, with no evidence in the literature of [U] at levels that indicate oxidized U in solution under these conditions. For instance, dissolution experiments in Callovo-Oxfordian simulated groundwater, presence of Fe(s) and Ar atmosphere of α-doped UO_2 fuel with alpha activity of 385 MBq/g, show low uranium concentrations being limited by $UO_2{\cdot}2H_2O$ (am) (Odorowski *et al.*. 2017). The same understanding is obtained from experiments of alpha doped UO_2 in presence of Fe(s) from Ollila and co-workers with total uranium concentrations $<10^{-10}$ M (Ollila *et al*. 2003, Ollila and Oversby 2005, Ollila *et al.* 2013; Evins *et al.* 2014). Small amount of sulphide can also supress any oxidizing effects of alpha activity (Ollila, 2006).

Similar results are obtained from leaching experiments of $U_{0.73}Pu_{0.27}O_2$ (alpha activity of 2200 MBq/gUO_2) in COx (Callovo-Oxfordian clay formation) simulated water-saturated in the presence of pre-corroded iron foil, showing the inhibition of the oxidative dissolution of the unirradiated MOX fuel due to the presence of iron and precipitation of magnetite on the MOX pellet surface, this can be partly attributed to consumption of H_2O_2 through oxidation of Fe(II) (Evins *et al.*. 2021).

The leaching behaviour of unirradiated Mimas® MOX fuel pellets containing an average of 7.48 wt% of PuO_2 (alpha activity of 1300MBq/gUO_2), with a heterogeneous microstructure containing Pu-rich agglomerates has also been studied under environmental conditions of increasing complexity (Jegou *et al.* 2022). The results indicate a decrease of three orders of magnitude of the uranium concentration in COx water compared to carbonated water (from $8.3{\cdot}10^{-5}$ to $7.3{\cdot}10^{-8}$ M) and the presence of Fe(II) further decreases the [U] to levels in equilibrium with UO_2(am). Interestingly, the pellet zone with the lowest Pu content and, therefore, low alpha activity, are the most sensitive to oxidative dissolution, being indicative of a possible Pu protective effect (Jegou *et al.* 2022).

4.2 Cr/Al-doped UO_2.

The incorporation of Cr and Al in the UO_2 fuel matrix modulates the microstructure triggering grain growth during sintering of the UO_2 pellets and minimizing FGR) (Arborelius *et al.* 2006; IAEA, 2010). The incorporation of dopants might affect the electrochemical properties of the matrix (He *et al*. 2007; Razdan and Shoesmith, 2013). To study the effect of Cr + Al dopant and particle size in the dissolution behaviour of irradiated fuel pellets in DGR, UO_2 samples with a range of doping level have been studied under different solution conditions in the framework of DisCo EU-project (Evins *et al*. 2021).

The obtained results seem to indicate the diminishing effect of Cr on the dissolution of UO_2 matrix, only identified when the conditions are mildly oxidizing (with traces of oxygen) or under H_2 pressure. The corrosion process has not been identified to be different from that occurring in pure UO_2. Consequently, Cr is not expected to have any significant influence on corrosion of irradiated spent fuel under the reducing conditions expected by the presence of corroding iron.

The main results from Cr/Al-doped UO_2 leaching experiments with different solutions and conditions are summarized below.

Oxidizing conditions in presence of H_2O_2

UO_2 and UO_2+Cr dissolution experiments were performed in bicarbonate solution using hydrogen peroxide to simulate the effect of oxidative radiolysis. The aim of the study was to investigate the influence of the microstructure in terms of porosity and grain size on the dissolution behaviour (Kegler *et al.* 2019, 2020). The results show no significant difference in the dissolution behaviour between Cr_2O_2 doped UO_2 and pure UO_2 pellets and, apparently, the pellet density (associated to the surface area) was more influent than dopant concentration (Evins *et al.*. 2021). Repeated exposures of UO_2 to hydrogen peroxide results in the formation of a thin layer of a secondary phase or hyperstoichiometric uranium oxide on the surface of the pellets (Maier *et al*. 2020; Li *et al.* 2023)

Air conditions

Under oxidizing, air-saturated conditions, in aqueous solutions with sodium chloride and bicarbonate, Cr-doped UO_2 dissolution results show a decrease of the initial dissolution rate with increasing Cr-

content. The different dissolution behaviour with the Cr level of doping is associated to the grain size, defect concentration and the Cr oxidation state, influencing to the oxygen vacancy formation (Smith *et al.*, 2020). A change of the Cr oxidation state is identified, from +2 for a content of 5-300 ppm to +3 with 600-2400 ppm of Cr (Evins *et al*. 2021).

Anoxic conditions

Under anoxic conditions the dissolution behaviour of 0.06 wt% Cr and 0.05 wt% Cr + 0.02 wt% Al doped UO_2 pellets was studied. The experimental conditions, described in Rodríguez-Villagra *et al*. (2022), are summarized herein. The tests were performed in autoclaves with hydrogen pressure containing Pt wire. The leaching solutions (carbonate solution with pH = 8.9 and young cement water with pH ~13.5) were stored in Ar glove box with a measured oxygen concentration of 1000ppm. The results indicate: i) leaching fresh doped-UO_2 solid samples in bicarbonate water did not apparently influence the evolution of the microstructure on the fuel surface and on the grain boundaries; ii) the presence of H_2 gas did not provide the expected reducing conditions considering its thermodynamic properties; iii) the combined effect of Cr and Al observed in Cr/Al-doped UO_2 seems to limit the uranium release in comparison with Cr-doped UO_2, in which Cr acts as a sole dopant (Rodríguez-Villagra *et al*. 2022; Rodríguez-Villagra *et al*. 2025).

Hydrogen pressure

Under hydrogen pressure (10bar hydrogen and using Pd/Pt as catalyst, placed in the headspace of the autoclaves, not immersed in the solution), Cr-doped UO_2 and UO_2 in YCWCa (pH = 13.5) leaching experiments show U concentration after 150 days of ~10^{-8} M and ~10^{-7} M, respectively. Therefore, Cr-doping diminished a factor of 6 the U release in YCWCa. Under the same reducing conditions and bicarbonate solution (pH = 9) the effect of Cr doping is less significant (Cachoir *et al.* 2021). Furthermore, Cr-doped UO_2 pellets seems to be less sensitive to the exposure to oxygen traces, being more resistant against oxidation or preventing the release of U(VI) from the surface at the start of the leaching tests.

Presence of Fe(s)

Under reducing conditions using Fe(s) as a reducing agent, the U concentration in the leaching experiments of UO_2 and Cr-doped UO_2 resulted to 10^{-11} M with no observed effects of the Cr-doping. (Evins *et al*. 2014; 2021).

4.3 REE-doped UO_2

The lanthanide (Ln) element group (Z = 57–71) predominates as trivalent cations and together with scandium (Z = 21) and yttrium (Z = 39), revealing related chemical properties with the Ln, all of these elements are categorized as the rare earth elements (REEs) (Evans, 1990). The incorporation of trivalent lanthanides and rare-earth (REE(III)) elements generated by the nuclear fission, such as Gd and Eu, in UO_2 matrix promotes the formation of oxygen vacancies clusters and stabilises this formation by maintaining the electroneutrality of the uranium oxide structure (Kim, 2001; Lee *et al.*., 2017; Park, 1992; Razdan & Shoesmith, 2014; Scheele *et al.*. 2021). In general, REE(III) elements with increasing doping content hinder the UO_2 oxidation to U_3O_8 (McEachern *et al.*, 1998; Scheele *et al.* 2004; Pehrman *et al.*, 2012; Razdan & Shoesmith, 2014; Olds *et al.* 2020; Scheele *et al.*, 2021), also seen in irradiated SNF (Milena-Pérez *et al.*, 2024) with enhanced oxidation resistance in the rim area. However, less knowledge is still acquired about the role of REE fission products in the SNF on aqueous dissolution process (Asmussen *et al.*, 2021). As discussed in section 2.2.3, trivalent rare-earth dopants (RE^{III}) also play an important role in slowing down the oxidative dissolution process of UO_2 matrix (He *et al.*, 2007; Razdan & Shoesmith, 2014; Casella, 2016; Barreiro, 2019). For of 4.5 wt% Gd doped UO_2 pellets the long-term dissolution rates under H_2 pressure were estimated as $3{\cdot}10^{-5}$, $9{\cdot}10^{-5}$ and $9{\cdot}10^{-7}$ $mol{\cdot}m^{-2}{\cdot}d^{-1}$ in perchlorate water, bicarbonate solution and YCW solution, respectively (Rodríguez-Villagra *et al*. 2020; Rodríguez-Villagra *et al*. 2025). The influence of Gd^{III} doping on the surface oxidation of UO_2 has been investigated in istu by XPS under 60, 200 and 350ºC and presence of hydrogen, argon or synthetic air streams saturated with water (García-Gómez *et al.* 2023a). The results indicate that the pellet porosity

is an important parameter to considerer when studying the surface oxidation of UO_2 doped with Gd_2O_3 as in these samples the oxidation depends on the atmospheric conditions. However, in absence of porosity doping UO_2 with gadolinia inhibit the UO_2 oxidation process (García-Gómez *et al.* 2023a).

Dissolution rates of Gd_2O_3 doped UO_2 (5 wt% and 10 wt%) in the presence of O_2 and bicarbonate were determined as a function of pH (9–13) using single pass flow-through (SPFT) system (García-Gómez *et al.* 2023b) resulting in rather low dissolution rates. Specifically, dissolution rates of Gd_2O_3-doped UO_2 at pH below 10 were found to be about 15 times lower than those of non-doped UO_2. Similarly, Asmussen *et al.*, (2024) studied the impact of Ce, Nd or Yb (1 - 5 at%) on the UO_2 dissolution using SPFT system under air conditions, observing lower dissolution rates on most samples relative to pure UO_2 samples. Experiments with UO_2 pellets with 1 wt% of Y_2O_3 under 10 mM HCO_3 and 0.2mM H_2O_2 solution showed a decrease in oxidative dissolution by a factor of 3.3 and 5.3 under inert and hydrogen atmosphere, respectively (Trummer *et al.*, 2010).

As mentioned, data on the effect of REE(III) (*e.g.* Sc, Y, La, Ce, Pr, Nd, Eu) on long-term behaviour of SNF remain limited and not fully understood, given the discrepancies found. Therefore, understanding the precise role of all fission products with variable compositions on SNF matrix dissolution under both oxidative and reducing conditions is necessary to strengthen predictive models, knowing that dissolution rates are highly conditioned on fuel composition and the presence of REE(III). Simplified model materials to study each REE independently could be used to avoid the chemical complexity of SIMFUEL and to understand the diverse chemical behaviour of fission products.

4.4 Zr-doped UO_2

With burnups beyond 40 MWd/kgHM, the initially open gap between fuel and cladding is closed leading to the formation of a fuel-cladding interaction layer. In the context of pellet-cladding interaction (PCI) phenomena, the behaviour under storage conditions of the UO_2-ZrO_2 inter-diffusion layer is characterized to be composed of two zones, one closer to the cladding (polycrystalline ZrO_2) and a second one nearer the fuel pellet mainly formed of solid solutions of $(U,Zr)O_2$ (cubic fluorite) (Frost, 2020). Various fission products such as iodine, caesium or tellurium attacks the cladding. Actually, stress corrosion cracking (SCC) induced by halogens, *e.g.* iodine, bromine and chlorine is responsible of cladding failures (König *et al.*, 2024). Despite all elemental halogens are able to induce SCC or pitting corrosion processes with the cladding material, chlorine and fluorine are impurities within the fuel, resulting from manufacturing processes and only iodine and bromine are generated by fission in sufficient amounts to enable cladding attack (Götzmann and Heuvel, 1979). Thermal analysis on some representative model materials of PCI showed that, under non-isothermal systems, the presence of zirconium in the UO_2 fuel matrix hinders matrix oxidation and the increase content of ZrO_2, decreases the fuel matrix oxidation degree (Rodríguez-Villagra *et al*. 2023; Vlassopoulos *et al*. 2024). The intimate U and zirconia layer may also include traces of volatile fission products that reach the gap. The behaviour and release of fission products and gaseous/volatile species will be influenced by PCI. However, the potential chemical resistance to oxidative dissolution/corrosion for long-term stability after disposal should be addressed. Certain experiments referred to fuel debris, particularly after Chernobyl and Fukushima Daichii accident, have been performed on $(U,Zr)O_2$-based simulated fuel debris under specific conditions non typical of DGR such as nitric acid, oxalic acid, malonic acid, artificial seawater (Sasaki *et al.*, 2014; Ikeuchi *et al.*, 2014; Kirishima *et al.*, 2022;Tonna *et al.*, 2023; Tonna *et al.*, 2024). Therefore, the research on PCI is still a high interest topic with considerable consequences at long-term storage that should be initiated by performing leaching experiments on surrogates of PCI (Zircaloy cladding) under DGR conditions.

5. Modelling radionuclides release from SNF

With the aim to predict the response of the system towards changes of individual parameters or events, one of the critical points for licensing SNF disposal is the need to mechanistically understand the

behaviour of SNF dissolution and its evolution under DGR conditions. For this purpose, efforts to simulate the spent fuel evolution under disposal conditions have resulted in the development of different modelling approaches in terms of complexity and simplification of the processes. A description of the mostly used models is reported Spahiu (2021). This section includes the latest development and improvements in the applicability and performance of these models.

5.1 Mechanistic models of radionuclides release during SNF leaching

In general, it exists in the literature two types of spent fuel dissolution models: chemical and electrochemical models. Both types of models consider the same fundamental processes occurring in the spent fuel matrix: non-oxidative dissolution, leading to U(IV) species, and the oxidative dissolution, leading to U(VI) species. However, the electrochemical models estimate the corrosion potential at the surface of SNF from the simulated concentration of radiolytic redox active species while the chemical models are based on redox processes to simulate the spent fuel oxidation and the calculated redox active species are used in the kinetic surface reactions of the redox processes. In any case, rate constants are determined either by oxidative dissolution experiments or by the extrapolation of measured current–potential relationships (Hossain *et al.*. 2006; Ekeroth and Jonsson, 2003; Shoesmith *et al.*. 2003; King and Kolar, 1999; Eriksen *et al.*. 2012).

Herein we include a description of the main characteristics of the models currently published in the literature, specifying if the model has been calibrated using experimental data and if it has been tested to reproduce independent experimental data (not used in the calibration of the kinetic processes) .

Matrix alteration model (MAM)

Matrix alteration model (MAM) developed in the framework of the Spent Fuel Stability European project (2000 -2004) (Poinssot *et al*. 2004) as a radiolytic model with a set of kinetic processes implemented in ChemSimul (Kirkegaard and Bjergbakke, 2002). The kinetic constants for the UO_2 oxidative dissolution mechanism were calibrated with experimental data (Merino *et al*. 2005). Subsequently, in the framework of the MICADO European project in collaboration with CIEMAT and ENRESA (Grambow *et al.*, 2011) and in several other projects in collaboration with ENRESA, the model was improved with the implementation of other important processes: the non-catalysed decomposition of hydrogen peroxide, activation of H_2 by epsilon particles and the reducing effect of the activated H_2 on the oxidized surface (Duro *et al.*. 2009; 2013).

Spent fuel dissolution model developed by AMPHOS 21

In the framework of the DisCo project, the MAM model kinetic processes were implemented in iCP (Nardi *et al.* 2014) and calibrated with experimental data (Cera *et al.* 2006; Evins *et al*. 2014). This implementation integrates the complete water radiolysis system from Kelm and Bohnert (2004) (based on 36 kinetic reactions) and its effect on the UO_2(am,hyd) alteration under container conditions in a 1D model. The most important feature of the described model is having solved the great challenge of: i) coupling radiolysis with reactions of chemical complexation and dissolution/precipitation processes which occur at very different time scales, often with rates differing by more than 6 orders of magnitude and ii) integrating these two systems: uranium (as the main element of the fuel) and the iron of the steel-container and metallic insert, which have a very complex chemistry (Riba *et al.*, 2020). The different physico-chemical processes implemented in the model are shown in Figure 5.1 and they are integrated iCP is achieved by a two-way coupling approach. The effect of water radiolysis on the UO_2(am,hyd) alteration is accounted by coupling H_2, O_2 and H_2O_2 generated by radiolyis to the kinetic process occurring on the UO_2 surface. The estimated UO_2 dissolution rates when including the effect of iron are of 0.6 $pmol \cdot m^{-2} \cdot s^{-1}$ (the same order of magnitude of the rates calculated in Wu *et al*. (2014b). The model

has allowed to simulate different sets of experimental data generated in the framework of DISCO EU-project (Riba *et al*. 2021).

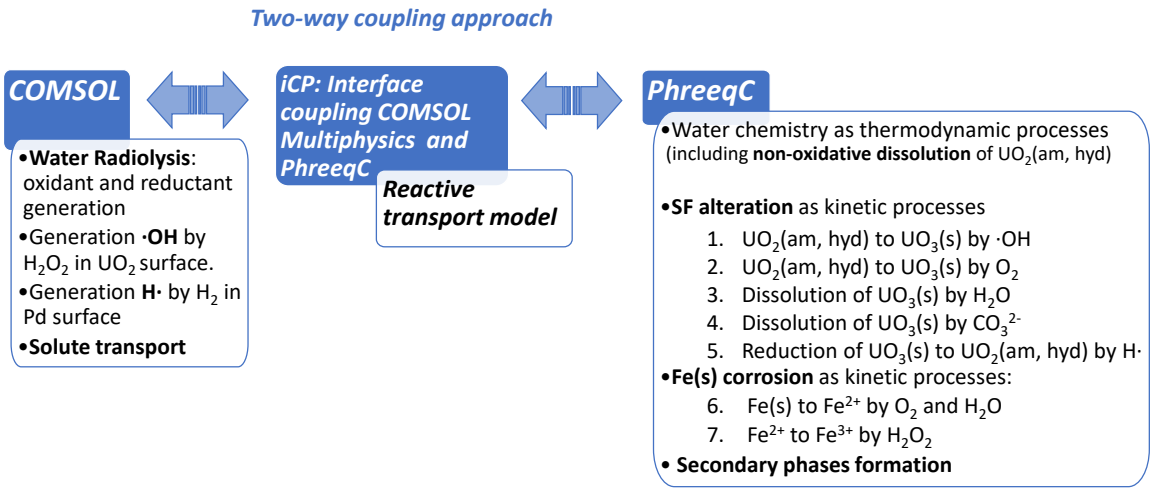

Figure 5.1. Integration in iCP of the different processes involved in the SF alteration.

CEA model

In the framework of the MICADO EU-project (Grambow *et al*. 2011), two different models from CEA (operational and radiolytic) were involved in the comparison exercise. The operational source term model considers primary radiolytic species produced in a water layer adjacent to the fuel surface and neglects conservatively reducing species and recombination of radicals. It assumes that 50% of the oxidizing species will contact the fuel surface instantaneously resulting to the oxidative dissolution of the fuel as U(VI). Secondary phase formation, reaction kinetics and the effect of hydrogen are neglected. It is a mass balance approach without fitting parameters. The CEA radiolytic model cannot be used for long-term calculations. It includes the complete radiolytic model and considers dose gradients and diffusion of species.

The oxidative dissolution of spent fuel UOx in a disposal cell has been implemented in HYTEC by De Windt *et al.*, (2003, 2006). The model included radiolytic-enhanced corrosion and long-term solubility-controlled dissolution of UOx, corroded C-steel canisters, bentonite backfills and a clayey host-rock (De Windt *et al.*, 2006).

In the framework of the DisCo EU-project (Evins *et al.* 2021), CEA modelling was focused on the simulation of non-irradiated homogenous MOX pellet ($U_{0.73}Pu_{0.27}O_2$) using the geochemical code CHESS with ThermoChimie database and coupled to HYTEC. The model includes: i) the rate of alpha-radiolytic production of H_2O_2; ii) disproportionation of H_2O_2 at the MOX pellet surface, iii) kinetics of the oxidative dissolution of the MOX matrix by H_2O_2; iii) the kinetics of reducing dissolution of the MOX matrix; and iv) the kinetics of anoxic corrosion of the iron foil, in synthetic COx claystone groundwater. In Figure 5.2 is shown a scheme with the coupled reactions considered in model. The model was upscaled to a simplified configuration of a generic disposal cell of cell MOX fuel assemblies in clay rock (De Windt *et al*. 2021).

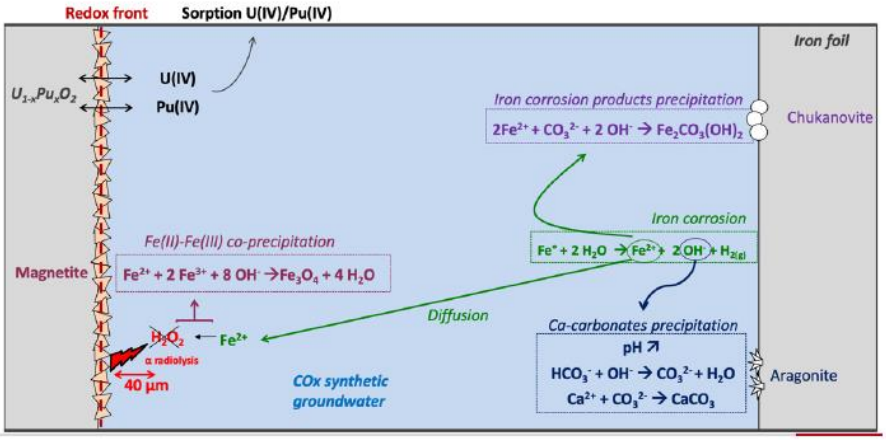

Figure 5.2. Coupled reactions taken into account in the reactive transport modelling of the homogeneous MOX alteration in synthetic Cox porewater in the presence of metallic iron. Figure from De Windt et al. (2021).

Spent fuel model developed by SUBATECH

SUBATECH model included in the comparison exercise of MICADO EU-project (Grambow *et al*. 2011) considers water radiolysis and diffusion of species. The radiolysis scheme is calculated with Maksima code and the effect of dose gradients at the fuel surface is implemented in the radiolytic transport code Traramo (Lundström, 2003). The coupling between the water radiolysis model and the surface reactions of the spent fuel is performed by electrochemical reactions. The effect of hydrogen is described by an effect of H_2 on the corrosion potential.

Thermodynamic modelling of spent fuel dissolution in a failed canister developed by PSI

PSI developed a batch model to describe the chemical evolution inside a failed spent fuel canister after saturation with porewater infiltrated from the bentonite buffer in contact with spent fuel or vitrified waste (Curti, 2021, 2022; Curti *et al*. 2023). In these models the potential effect of water radiolysis on the fuel oxidation is assumed to be insignificant based on the consideration that molecular hydrogen from canister corrosion is expected to protect the fuel surface from radiolytic oxidation. The batch thermodynamic calculations are performed using TDB2020 database (Hummel and Thoenen, 2023). Aqueous and solid speciation are determined by equilibrating kinetically scaled amounts of the interacting materials (fuel, encasing structural materials and carbon-steel canister) with bentonite porewater filling the canister cavity. The calculations were performed assuming either unconstrained (chemical system inside the canister is assumed to be closed to transfer of CO_2 (and also H_2) to or from any external reservoir) or externally imposed pCO_2, equal to the bentonite porewater.

Fuel Matrix Dissolution Model (FMDM)

The FMDM is a one-dimensional reaction–diffusion model (Jerden *et al.* 2015) integrating the process scheme of Figure 5.3 implemented in MATLAB code. The mathematical representation of the system shown in Figure 5.3 involves a set of coupled partial differential equations (one for every component), which are solved as a fixed-boundary problem by the electrochemical approach employed by King and Kolar (1999) in the original MPM (King and Kolar, 1999; 2002; 2003; Shoesmith *et al.*. 2003). The most important results are i) hydrogen oxidation half reaction balances the hydrogen peroxide reduction reactions to lower the corrosion potential and ‘‘protect’’ the fuel from oxidative dissolution at even submillimolar concentrations, ii) hydrogen concentrations greater than 0.1 mM, the hydrogen effect

shuts down oxidative dissolution of the fuel, even in the presence of 1 mM carbonate, iii) The presence of a U(VI) precipitate/corrosion layer consisting of schoepite and/or studtite can decrease the dissolution rate of the fuel by a factor of two or more depending on the porosity of the layer.

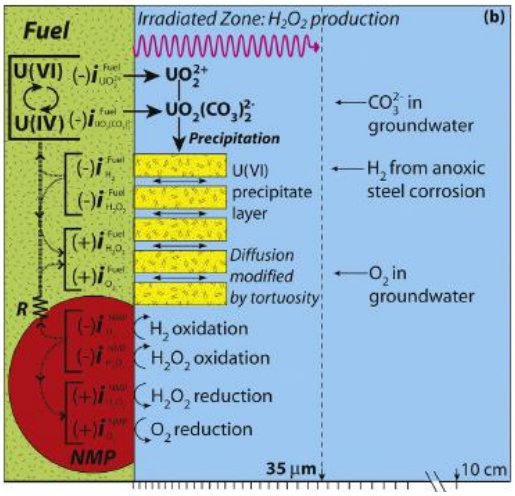

Figure 5.3. Summary of the FMDM reaction current paths and model layout with a surface layer. Figure from Jerden et al. (2015).

Model of UWO

The model of UWO (University of Western Ontario, Canada) used a one-dimensional model implemented in COMSOL Multiphysics, with diffusion-reaction expressions solved numerically by finite element methods (Wu *et al*. 2012, 2014a, 204b). The preliminary model (Wu *et al*. 2012) is based on a series of homogeneous and heterogeneous reactions to determine the influence of redox conditions on the radiolytic corrosion of spent fuel. The model predicted that the corrosion of UO_2 could be suppressed by the steel corrosion products, Fe^{2+} and, in particular, H_2.

The updated version of the model (Wu *et al*. 2014a) included: (1) a complete reaction set for the α-radiolysis of water including the generation of, and the interactions between, the radiolysis products; (2) the oxidative dissolution (corrosion) of UO_2 driven by H_2O_2 reduction on both the UO_2 surface and noble metal particles; (3) the reduction of oxidized surface species (UV/UVI) by H_2 oxidation on noble metal particles and of dissolved UO_2^{2+} either by reaction with H_2 in solution or with H_2 catalysed on the fuel surface; (4) the reaction of H_2O_2 with H_2 catalysed by noble metal particles; (5) the scavenging of H_2O_2 in homogeneous solution by reaction with Fe^{2+}; and (6) the decomposition of H_2O_2 to O_2 and H_2O.

Furthermore, a two-dimensional model (Wu *et al*. 2014b) has been developed showing that a simplified α-radiolysis model which only accounts for the radiolytic production of H_2O_2 and H_2 provides a reasonably accurate simulation. This conclusion is derived from the comparison of the calculated temporal evolution of the radiolytic species considering the radiolytic scheme also used in other models (Elliot and Bartels, 2009; Joseph et al. 2008) and the concentration of H_2O_2 and H_2 estimated from the dose rate and the primary yield. The developed 2D model (Wu *et al*. 2014b) was modified to be applied to simulate the influence of the redox processes occurring within fractures in SNF (Liu *et al*. 2016; 2017). Calculations of corrosion rates for α-doped UO_2 in a closed system demonstrate that the accumulation of O_2 lead to an increase in corrosion rate. Even though the rate constant for the reaction of O_2 is ~200 times less than that of H_2O_2, the effect of O_2 can be significant since the steady-state [O_2] can be greater than that of H_2O_2 in a closed system. However, under the influence of radiolytic H_2, the α-doped UO_2 corrosion rates decrease with time to insignificant values ($<10^{-20}$ mol·m^{-2}·s^{-1}). The influence of the temperature and the flow conditions on the UO_2 corrosion have been quantified with pore-scale transport

2D model (Liu *et al.*. 2020) and 3D model (Liu *et al.*. 2023) considering non irradiated UO_2 pellet and coupling thermal advection and conduction with chemical reactions.

KTH models: Steady state and mechanistic model

In any system where reactive species are produced at a constant rate, steady-state will eventually be reached. At this point, the rate of production of reactive species is balanced by the rate of consumption of these species in the system. The KTH steady state model is based on the conservative approach that the rate of UO_2 oxidation equals the rate of radiolytic oxidant production (at constant dose rate). In a system where dissolution of U(VI) is not hindered, the rate of dissolution is assumed equal to the rate of UO_2 oxidation. Assuming that radiolytic oxidants are only consumed in reactions with UO_2, the steady state approach yields the maximum dissolution rate that can be attributed to water radiolysis. The approach is further simplified to include only H_2O_2 as the active UO_2 oxidant on the basis that the relative impact of H_2O_2 amounts to > 99.9 % of the total oxidation potential (Ekeroth and Jonsson, 2003; Jonsson *et al.*. 2007, Roth and Jonsson 2008). Hydrogen effects are described by catalytic interaction with the epsilon phases involved in the reactions: i) H_2 with H_2O_2 (Nilsson and Jonsson, 2008a), ii) H_2 with aqueous U(VI) (Nilsson and Jonsson, 2008b, iii) reduction of oxidized UO_2 on SNF surface (Broczkowski *et al.*. 2005; Trummer *et al.*. 2008; Eriksen *et al.*. 2008). The model predicts that only 0.1 bar H_2 will effectively inhibit the dissolution of the spent fuel aged 100 years or more, while in the presence of 1 µM Fe^{2+}, even 0.01 bar H_2 will be sufficient to stop oxidative fuel dissolution (Jonsson *et al.*. 2007).

The KTH model participated in the comparison exercise of MICADO EU-project (Grambow *et al*. 2011), accounting for the process of water radiolysis and diffusion of species and heterogeneous kinetics at the SF surface.

Recently, a mechanistic 1D model, coupling kinetics of surface mediated reactions and diffusion in, has been developed in MATLAB code (Hansson *et al*. 2023). The model performed simulations using the full reaction set and a simplified system accounting only for H_2O_2 production in the aqueous phase are in reasonably good agreement regarding the evolution of H_2O_2 and U(VI)(aq) concentrations. Surface site reaction system accounts for the experimental observations of surface-bound hydroxyl radical as well as the formation of U(V) in the oxidative dissolution reaction with the implementation of: i) the reaction between H_2 and the surface-bound hydroxyl radical, preventing the UO_2 oxidation; and ii) U(VI) reduction on the surface of UO_2 by H_2 ε-particles catalysed, being the latter the most efficient one (Hansson and Jonsson *et al*. 2023).

SERNIM model developed by UPC

The Segregated Radionuclide Identification and Quantification Model (SERNIM) is a semi-empirical model developed to determine the relative importance of the contribution from different sources on the total release of a radionuclide. The main objective is to determine how much radionuclide is released to the solution from the SNF discerning from pre-oxidized phases or fines, matrix dissolution, phases segregated from the matrix and IRF contribution (Espriu-Gascon *et al.*. 2020; Iglesias *et al.*. 2023). The model is based on two assumptions.

1) The total amount of a radionuclide release at any time is the sum of the release of the radionuclide from its different locations in the fuel. The model does not take into account any secondary phase precipitation after the dissolution process.
2) The release of the radionuclide from each source follows first order kinetics.

The mathematical expression derived from these assumptions is represented below:

$$m_{RN}(t) = \sum_{c=1}^{N} m(c)_{RN,\infty} \cdot \left(1 - e^{-k_c t}\right)$$

Where "$m_{RN}(t)$" is the number of cumulative moles of radionuclide released as time t, (in moles), "$m(c)_{RN,t=\infty}$" is the number of radionuclide moles released from contribution "c" at infinite time, "k_c" is the rate constant for the release of the radionuclide from the "c" contribution (in day), and "t" is time (in day). The sources of radionuclide "c" normally considered are: '"ma" matrix, "ox" pre-oxidized phases and "seg" grain boundaries and gap (seg).

5.2 Fuel performance and FGR modelling

Approximately 30% of the generated fission products during normal reactor operations are noble gases (Xe and Kr) poorly dissolved in the UO_2 matrix and, consequently, they are accumulated as gas bubbles (Olander, 1976; Cacuci, 2010). Many fuel performance codes have implemented empirical correlations to describe materials properties and FGR distribution in irradiated fuel rod.

In Pękala *et al*. (2013) the empirical observations included in models are discussed, such as the correlation of the FGR with the linear heat generation rate and the burn-up degree for BU > 40 GWd/tiHM (Kamimura, 1992; Spino, 1998), over which the formation of a rim structure is evidenced, acting as a sink for Xe for accumulation (Johnson *et al*., 2005). In agreement with these previous findings, a review of models and experiments conducted by Guo *et al*. (2022) concluded that most enhancing factors of the fission gas release are, for most of the fuels, burn up, time and temperature. In a variety of fuels, Xe diffusion coefficient will decrease with temperature until it reaches a stable value.

A brief description of the mathematical expressions of these phenomena is included in Pękala *et al*. (2013) referencing other works (Booth, 1957; Blair, 2008; Van Uffelen, 2002; Pastore *et al*., 2013). As described in Tonks *et al*. (2018) the release of fission gas occurs through three distinguished steps:

i) Fission gas production and bubble mobility through the bulk of the grain (a complete review on bubble mobility is given in Veshchunov, 2008), bubble growth (Lösönen, 2000), bubble re-solution (MacInnes and Brearley, 1982; Olander and Wongsawaeng, 2006; Pastore *et al*., 2015)

ii) Grain phase bubble nucleation, growth and interconnection with grain edge bubbles (White and Tucker, 1983; 1994; White, 2004; Veshchunov, 2008; Rest, 2003; Olander and Van Uffelen, 2001).

iii) Transport of gas through interconnected grain edge tunnels to free surfaces for release (Turnbull, 1974; Turnbull and Friskney, 1987; Turnbull and Tucker, 1974)

Rest *et al*. (2018) published a review of the basic mechanisms of fission gas release during normal reactor operation including recommendations for future work structure in the different areas (bulk diffusivity, bubble nucleation and re-solution, thermal conductivity and gas concentration at grain boundaries. The authors include a valuable set of key points summarising the behaviour of fission gas in high burn-up structure.

The calculation of fission gas generation, transport and release is generally included in fuel performance assessment codes. A description of the mostly used fuel performance codes for the simulation of in-reactor fuel behaviour and in predisposal/disposal activities is available in Vlassopoulos *et al*. (2024) EURAD WP8: Spent Fuel Characterisation and Evolution Until Disposal updated SOTA Report. The report includes not only a revision of the depletion codes but also an update of the improvement in the

accuracy and validations of these codes using new experimental techniques and data, achieved during SFC WP8 of EURAD project.

Despite FGR models implemented in fuel performance codes focus on the release under reactor operation conditions, they provide value information on the release of radionuclides under repository conditions. Furthermore, the correlation between FGR and IRF has been empirically demonstrated (Johnson *et al*., 2004; 2005; Johnson and Tait, 1997; Johnson and McGinnes, 2002; Lassmann *et al*., 2000; Casas *et al*. 2012; Lemmens *et al*. 2017). Consequently, the quantification of the FGR is highly valuable for the determination of the release of some fission products upon contact with groundwater under repository conditions. Based on the evidenced correlation between IRF and FGR, full-core fuel performance calculations have been suggested as a tool for estimating IRF in separate fuel assemblies (Johnson *et al*., 2004; 2012). However, as the manufacturing parameters are not accurate but subject to specific error margins, calculations with nominal manufacturing parameters will lead to non-conservative or excessively conservative estimates. To take uncertainty of the input parameters into account, Wilks' order statistics can be applied for FRAPCON fuel performance calculations (Wills, 1942; Glaeser, 2008).

Tonks *et al*. (2018) review the recent improvements on the understanding of the fission gas production, transport and release during normal reactor operation, underpinning the remaining open questions with suggestions on how address these uncertainties.

Some codes have been particularly developed for FGR analysis, as it is the case of meso-scale model of irradiated UO_2 fuel behaviour and fission product release (MFPR) (Veshchunov *et al*., 2006; 2007) and SFPR code (Veshchunov *et al*. 2011; 2015) for mechanistic modelling of single fuel rod behaviour under various regimes of LWR operation (normal and off-normal, including accident).

The MFPR is able to quantify: i) the influence of microscopic defects of the UO_2 structure such as vacancies, interstitial and fission atoms, bubbles, pores and dislocations on the transport of fission gases; ii) inter-granular bubble mobility considering volume diffusion, bubble evaporation/condensation and surface diffusion; and iii) grain face transport of gas atoms incorporating the effect of atom diffusion, trapping and irradiation- induced re-solution (Veshchunov *et al*., 2007; Veshchunov and Shestak, 2008; Veshchunov and Tarasov, 2009; Tarasov and Veshchunov, 2009).

The SFPR meso-scale models include an extended set of microscopic parameters, characterizing the crystal defect structure, thermo-physical and thermo-chemical properties of irradiated fuel. Such multi-scale simulations of the key microscopic parameters are based on atomic scale physics, allowing to predict the macroscopic characteristics of the irradiated fuel and cladding such as cracking, porosity and grain size (Veshchunov *et al*. 2015). A state-of-the-art knowledge of micro-mechanical fuel performance is presented in Michel *et al*. (2024).

Molecular dynamics simulations have been widely adopted to study the behaviours of fuels and fission gas at the atomic scale (Moore *et al*. 2011; Liu and Andersson, 2015; Xia *et al*. 2022; Galvin *et al*. 2021; Guo *et al*. 2025), including point defects (Wang *et al*. 2022), dislocations (Lunev *et al*. 2018), grain boundaries (Chiang *et al*. 2014; Borde *et al*. 2021), Xe atoms and Xe bubbles (Deng *et al*. 2014; Cooper *et al*, 2016; Xiao-Feng *et al*, 2010).

FRAMATOM FGR model simulations (implemented in the COPERNIC fuel performance assessment code) has been compared with a database of experimental data of 400 rods covering high burn-ups, high powers, short to long transients, UO_2, UO_2-Gd_2O_3 and MOX fuels showing the capacity of FGR models to reproduce experimental data (see Figure 5.4) (Bernard *et al.*. 2000).

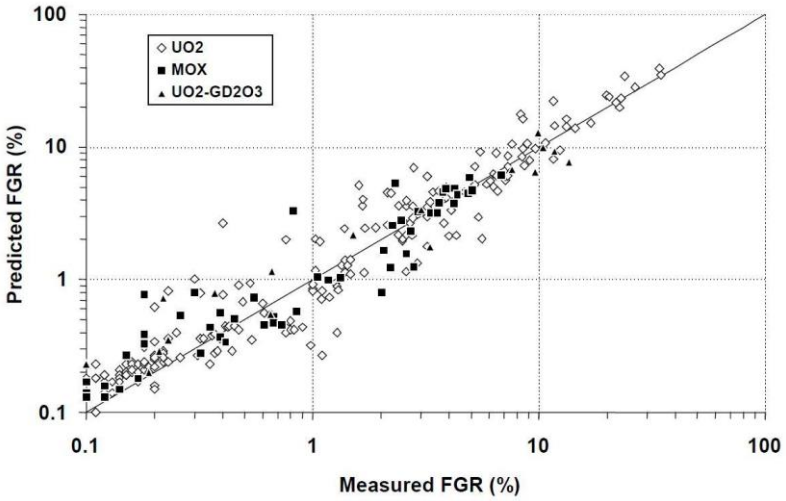

Figure 5.4. Validation of the FRAMATOM FGR steady-state model against experimental data (Figure from Bernard et al. 2000).

Other codes, such as FASTGRASS, developed by NRC (USA), has the capability to simulate the migration of not only fission gases but also volatiles fission products (I, Te, Cs) and alkaline earth elements (Sr and Ba) (Rest and Zawadzki, 1992)

Simulations based on statistical physics concepts, such as the phase-field theory, have been successfully applied to modelling the 3-D structure evolution of irradiated fuels. Li and co-workers (2012a, 2012b) developed a phase-field model to simulate gas atom segregation at grain boundaries and the effect of interfacial energy and gas mobility on gas bubble morphology and growth kinetics in a bi-crystal UO_2 during post-irradiation thermal annealing (Li *et al*. 2012b). The application of phase-field models has the potential to reduce many of the simplifying assumptions used to calculate the gas deposition rate at grain boundaries.

Pastore *et al*. (2018) describe the implementation in the BISON fuel performance code of the fission gas behaviour which couples fundamental physical processes of intra-granular bubble evolution and swelling with to gas atom diffusion, bubble evolution at grain boundaries, fission gas release due to grain-boundary bubble interconnection and micro-cracking during transients. The model is validated with experimental data of fission gas release and xenon radial distribution. Cunningham (2024) simulates also with BISON fuel performance code the impact of temperature, burnup and power on the fission gas release. The model solves the heat equation to calculate radial temperature distribution throughout the fuel pellet.

Recent advances have been published (Magni *et al*. 2023; Giaccardi *et al*. 2024) on the implementation of the inert gas behaviour in the meso-scale software SCIANTIX, for coupling with fuel performance codes (TRANSURANUS and GERMINAL). The model pairs rate-theory description of helium intra-granular behaviour (diffusion towards grain boundaries, trapping in spherical bubbles, thermal re-solution), developed in a first step, with rate-theory description of helium inter-granular behaviour (diffusion towards grain edges, trapping in lenticular bubbles, thermal re-solution) (Giorgi *et al*. (2021). Giaccardi *et al*. (2024) describes the development in TRANSURANUS to model radioactive gas and volatile fission products from defective fuel rods with a two-step approach (fuel-to-gap and gap-to-coolant release).

Numerical modelling of fission gas diffusion in oxidized fuel is necessary to evaluate fission gas diffusion when oxidation occurs in the nuclear fuel. The diffusivity of fission gas like Kr and Xe, is known to be higher in hyper-stoichiometric fuel (Rest *et al*., 2018). The released fission products may present different behaviours in the oxidized UO_{2+x} fuel (Colle *et al*., 2006; Cox *et al*., 1986; Massih, 2018). The effect of the grain boundary on UO_2 oxidation and fission gas diffusion has been simulated in a grain scale (pore-scale) model developed by Liu *et al*. (2020). In this method, simulation is conducted directly

on the images of the microstructure of materials. The thermal-chemical processes coupling heat conduction and oxidation are directly simulated on the images of the UO_2 fuel microstructures (Liu *et al*., 2021).

FGR models focussed on Cr-doped fuel are also used for benchmarking fuel performance code TRANSURANUS (Gonzalez and Ševecek, 2022). The work points out the need to fully understand the phenomena involved in adding Cr as a dopant in UO_2 on the thermomechanical properties.

6. Identified gaps and motivation for the current project

6.1 Instant release fraction

For IRF studies, further studies are warranted in the following areas:

The release of fission gases during autoclave leaching of SNF should be better understood. This is needed to better describe the relationship between FGR and IRF, which is commonly used in safety assessments to quantify the IRF of I-129, Cs-137 and Cs-135.

More data are needed regarding the effects of leaching environment and water chemistry on IRF from SNF. These data are needed to strengthen the safety cases for different repository environments.

Dopants in modern fuel types may affect partitioning of fission products which may influence the IRF. Some results from the ADOPT studies indicate that the Cr-Al doping will affect the IRF of certain radionuclides, meaning that how dopants affect the partitioning of radionuclides should be further studied.

The effects of fuel type, reactor operation and sample preparation can have huge effects on the results and this needs to be addressed in future endeavours to get a coherent picture of the radionuclide release, in particular the IRF.

The existing database with experimental data, from the FIRST-Nuclides project, should be improved and expanded in order to allow grouping of similar experiments. The current database was compiled in 2014 and contains mainly results from expeirments without initial hydrogen in the system. It is in an Excel format and available via the project website (www.firstnuclides.eu). In any effort to combine data from many experiments into a single database, care need to be taken to collect information of experimental detail and select comparable experiments before data are used for evaluating correlations or formulating models. International efforts are needed to populate this database with enough data to allow these valid data selections and still have enough data to provide significant results.

6.2 Release of RN from SNF matrix

For matrix release, further studies are warranted in the following areas:

For deep understanding of multiparametric systems and inter-comparison purpose between experimental data, the specific synthesis conditions of doped samples (including the cooling step) and the harmonization using a common leaching protocol should be provided.

How dopants influence the UO_2 surface with regards to the surface-mediated redox reactions involved in oxidative dissolution and the hydrogen effect need to better understood. For example, is there a difference between Cr+Al doped fuels and fuels with Cr as a single dopant?

Understanding of the Cr-doped spent fuel pellet structure both at atomic and micro scale to clarify the redox state of Cr, charge compensation mechanism and to the characteristic microstructure this type of materials.

Regarding the hydrogen effect, there is need to establish a full picture of the different potential reactions. This is needed for relating [H_2] with oxidative dissolution rate and dose rate.

The effect of iron-based materials on the oxidative dissolution: Fe corrosion and hydrogen production, secondary mineral formation and Fe in solution all have significant effect on the chemical environment in the near field.

There are still some unresolved questions and discussions concerning what is behind the doping effect seen by 3-valent elements in the UO_2 matrix. In addition, the observed effect of Th (4-valent) is not understood.

Results from model materials with highly mobile radionuclides (Cs, I) incorporated in the structure are also missing.

Currently demands on higher burnups, should consider the PCI without and with the presence of aggressive fission products released by the pellets (*e.g.* Cs and I) in fuel behaviour under long-term storage conditions, and perhaps, to stablish an empirical PCI criterion for high burnup fuel to be disposed into the DGR. This would require PCI experimental analysis using model materials.

Considering the likelihood that hydrogen can suppress the radiolytic oxidation of UO_2 in a repository environment, the non-oxidative dissolution rate in a repository perspective needs further attention.

For both IRF and matrix release, there is a need to improve and expand database with experimental data to allow grouping of similar experiments.

Understanding the processes that control radionuclides release from SNF is important for dose assessments in the repository setting. Hence, more data are needed on uranyl secondary phase's (formed during the oxidative alteration of SNF) stability, evolution and its retention capacity of radionuclides.

6.3 Effect of grain boundaries on the leaching behaviour

The actual radionuclide inventory residing in grain boundaries has proven hard to determine. Theoretically, it varies between fuels depending on burnup and temperature, but there is a dearth of experimental data to verify and quantify this fraction.

In general, there is a need to understand how grain boundaries participate in the dissolution process. For spent fuel leaching experiments, novel methods to separate the grain boundary release from the gap and the matrix are needed.

Improved knowledge of the character of grain boundaries, such as the lattice mismatch or degree of non-stoichiometry, combined with observed behaviour during leaching is an important complement to the spent fuel experiments.

Experiments using model materials with highly mobile elements (Cs, I) incorporated in the structure – fully or to some degree in grain boundaries – are also missing.

Analytical techniques that focus on the grain boundaries need to be explored, with regards to their various applications ranging from determining the content of segregated elements, to characterizing the grain boundaries crystallographically as well as observing their response to leaching.. More studies using for example FIB and TEM would improve the knowledge base regarding expected radionuclide release from grain boundaries.

6.4 Mechanistic models of SNF leaching

For the improvement of the mechanistic models the following areas need to be explored with the fundamental need to combine modelling and experimental efforts:

Improve knowledge on the impact of simplifying the radiolytic scheme considered in the SNF corrosion, such as the effect of considering only H_2O_2 in the oxidation of UO_2 (versus considering also the radiolytic

O_2) in dependence of simulating an open or closed system and the quantification of water radiolytic species in presence of chloride.

To distinguish between dissolution from the matrix, cracks, grain boundaries and the gap at scale of SNF pellet and to better quantify the effect of the gap and the high-burn-up structure in the instant release fraction and matrix dissolution.

Quantification of the effect of different amount of epsilon particles on the release of fission and activation products as well as matrix dissolution.

Interpretation or transposition at the DGR scale: which process(es) prevail in the different phases expected in repository conditions (e. g. Fe/H_2 effect).

Improvement on the mechanistic understanding of the process occurring in the spent fuel matrix surface with H_2O_2.

6.5 FGR modelling

Uncertainty estimations from fuel performance calculations related to FGR have not been taken into account while comparing experimental FGR and IRF in previous investigations. Including the whole chain from uncertainty of input parameters until the FGR/IRF experiments for the same rods in fuel performance analysis is one of the motivations on this topic for the current project.

References

Arborelius, J., Backman, K., Hallstadius, L., Limbäck, M., Nilsson, J., Rebensdorff, B., ... & Rönnberg, G. (2006). Advanced doped UO2 pellets in LWR applications. *Journal of Nuclear Science and Technology*, *43*(9), 967-976.

Asmussen, S. E., Asmussen, R. M., Goulet, A. P., Shimskey, R. W., & Hanson, B. D. (2024). The effect of cerium, neodymium, and ytterbium doping on UO_2 dissolution. *Journal of Nuclear Materials*, *591*, 154916.

Asmussen, S.E., Goulet, A.P., Hanson, B.D. (2021).Scoping Studies on the Effects of Dopants and Hydrogen on UO2 Dissolution Rates, PNNL-31733

Barreiro-Fidalgo, A., Roth, O., Puranen, A., Evins, L.Z. and Spahiu, K. (2021) in Evins *et al.*, DisCo Deliverable D1.25 Final meeting Proceedings, Grant Agreement: 755443.

Barreiro Fidalgo, A., Jonsson, M. (2019). Radiation induced dissolution of $(U,Gd)O_2$ pellets in aqueous solution – A comparison to standard UO_2 pellets, Journal of Nuclear Materials 514, 216-223.

Barreiro Fidalgo, A., Kumagai, Y., & Jonsson, M. (2018). The role of surface-bound hydroxyl radicals in the reaction between H2O2 and UO2. Journal of Coordination Chemistry, 71(11-13), 1799-1807.

Barreiro-Fidalgo, A., Roth, O., Evins, L. Z., & Spahiu, K. (2021). Aqueous leaching of Cr_2O_3-doped UO_2 spent nuclear fuel under oxidizing conditions. *MRS Advances*, *6*, 103-106.

Bauhn, L., Hansson, N., Ekberg, C., Fors, P., Delville, R., Spahiu, K., (2018). The interaction of molecular hydrogen with α-radiolytic oxidants on a $(U,Pu)O_2$ surface. J. Nucl. Mater. 505, 54–61.

Bernard L. C., Jacoud J. L. and Vesco P. (2000). FRAMATOME analysis of fission gas release and related topics. In: Fission gas behaviour in water reactor fuels. Seminar Proceedings, Cadarache, France 26-29 September 2000. Nuclear Energy Agency (NEA)

Blair, P. (2008). Modelling of fission gas behaviour in high burnup nuclear fuel. PhD Thesis, École Polytechnique Fédérale de Lausanne

Booth, A. H. (1957). A method for calculating fission gas diffusion from UO_2 fuel and its applications to the X-2-f loop test. AECL Report 496.

Borde, M., Germain, A., & Bourasseau, E. (2021). Molecular dynamics study of UO_2 symmetric tilt grain boundaries around [001] axis. *Journal of the American Ceramic Society*, *104*(6), 2879-2893.

Broczkowski, M., Noël, J., Shoesmith, D. (2005). The inhibiting effects of hydrogen on the corrosion of uranium dioxide under nuclear waste disposal conditions. J. Nucl. Mater. 346, pp. 16-23.

Cachoir, C., Mennecart, T., & Lemmens, K. (2021). Evolution of the uranium concentration in dissolution experiments with Cr-(Pu) doped UO 2 in reducing conditions at SCK CEN. *MRS Advances*, *6*, 84-89.

Cacuci, D. G. (Ed.). (2010). *Handbook of Nuclear Engineering: Vol. 1: Nuclear Engineering Fundamentals; Vol. 2: Reactor Design; Vol. 3: Reactor Analysis; Vol. 4: Reactors of Generations III and IV; Vol. 5: Fuel Cycles, Decommissioning, Waste Disposal and Safeguards* (Vol. 1). Springer Science & Business Media.

Carbol, P., & Spahiu, K. (2005). *The effect of dissolved hydrogen on the dissolution of 233U doped UO_2 (s) high burn-up spent fuel and MOX fuel* (No. SKB-TR--05-09). Swedish Nuclear Fuel and Waste Management Co..

Cardinaels, T., Govers, K., Vos, B., Van den Berghe, S., Verwerft, M., de Tollenaere, L., Maier, G. and Delafoy, C., 2010, January. Characterisation of Cr2O3 Doped Fuel. In Proceedings of the Enlarged Halden Programme Group Meeting (pp. 1-13). IFE.

Casas I., Espriu A., Serrano-Purroy D., Martínez-Esparza A. and de Pablo J. (2012). IRF modelling from high burn-up spent fuel leaching experiments. 1st Annual Workshop Proceedings of the 7th EC FP – First Nuclides, Budapest, Hungary 9-11 October 2012.

Casella, A., Hanson, B., Miller, W. (2016). The effect of fuel chemistry on UO_2 dissolution, Journal of Nuclear Materials 476, 45-55

CEA (2009) DEN Monograph, “Nuclear fuels”, Ed: J-F Parisot. CEA, Saclay and Groupe Moniteur (Éditions de Moniteur), Paris

Chiang, T. W., Chernatynskiy, A., Sinnott, S. B., & Phillpot, S. R. (2014). Interaction between voids and grain boundaries in UO2 by molecular-dynamics simulation. *Journal of nuclear materials*, *448*(1-3), 53-61.

Colle, J. Y., Hiernaut, J. P., Papaioannou, D., Ronchi, C., & Sasahara, A. (2006). Fission product release in high-burn-up UO_2 oxidized to U_3O_8. *Journal of nuclear materials*, *348*(3), 229-242.

Cooper, M. W. D., Middleburgh, S. C., & Grimes, R. W. (2014). Swelling due to the partition of soluble fission products between the grey phase and uranium dioxide. Progress in Nuclear Energy, 72, 33-37.

Cooper, M. W. D., Stanek, C. R., Turnbull, J. A., Uberuaga, B. P., & Andersson, D. A. (2016). Simulation of radiation driven fission gas diffusion in UO_2, ThO_2 and PuO_2. *Journal of Nuclear Materials*, *481*, 125-133.

Corkhill, C. L., Myllykylä, E., Bailey, D. J., Thornber, S. M., Qi, J., Maldonado, P., Stennett, M.C., Hamilton A. & Hyatt, N. C. (2014). Contribution of energetically reactive surface features to the dissolution of CeO_2 and ThO2 analogues for spent nuclear fuel microstructures. ACS applied materials & interfaces, 6(15), 12279-12289

Cox, D. S., Iglesias, F. C., Hunt, C. E. L., Keller, N. A., Barrand, R. D., Mitchell, J. R., & O'Connor, R. F. (1986). Oxidation of UO 2 in air and steam with relevance to fission product releases. In *American Chemical Society, Division of Nuclear Chemistry and Technology*.

Cunningham, K. (2024). *Modeling UO_2 and UN Fuel Fission Gas Release Instances in BISON for Microreactor Applications* (Doctoral dissertation, Massachusetts Institute of Technology).

Curti, E. (2021). Thermodynamic modelling of “inside canister” conditions during UO_2 spent fuel dissolution in a failed steel container. Deliverable D5.6, DISCO project, grant agreement 755443, Horizon 2020 Framework Programme, European Commission.

Curti, E. (2022): Aqueous corrosion of vitrified nuclear waste: Current process understanding, literature review and recommended rates. Nagra Arbeitsbericht NAB 23-09

Curti, E., Puranen, A., Grolimund, D., Jädernas, D., Sheptyakova, D., Mesbah, A., 2015. Characterization of selenium in UO_2 spent nuclear fuel by micro X-ray absorption spectroscopy and its thermodynamic stability. Environmental Science: Processes and Impacts, 17, 1760.

Curti, E., Thoenen, T., Kosakowski, G., Baeyens, B., Van Loon, L.R., Leupin, O.X. & Martin, L. (2023): The Geochemical Evolution of the Near-Field in the HLW Section of the Combined Repository at Nördlich Lägern. Nagra Technical Report 23-02.

De Windt, L., Burnol, A., Montarnal, P., van der Lee, J. (2003). Intercomparison of reactive transport models applied to UO_2 oxidative dissolution and uranium migration. Journal of Contaminant Hydrology 61, 303–312.

De Windt, L., Schneider, H., Ferry, C., Catalette, H., Lagneau, V., Poinssot, C., Poulesquen, A., Jegou, C. (2006). Modeling radionuclide source-terms and release in a spent nuclear fuel disposal. Radiochimica Acta 94, 787–794.

De Windt L, Goblet P, Kerleguer V, Jégou C, (2021). Modeling of $U_{0.73}Pu_{0.27}O_2$ radiolytic dissolution as a simulant of the alteration of MOX fuel matrices in an underground disposal cell. Deliverable 5.7, DisCo

project (Grant Agreement 755443), Euratom Research and Training Programme on Nuclear Energy, Horizon 2020 Framework Programme, European Commission.

Deng, B. L., Tian, X. F., Zhai, J., & Hu, Y. F. (2014). Effect of fission Xe on diffusion of oxygen and uranium in UO_2: a molecular dynamics study. *Indian Journal of Physics*, *88*, 1183-1189.

Duro, L., Riba, O., Martínez-Esparza, A., Bruno, J. (2013). Modelling the activation of H_2 on spent fuel surface and inhibiting effect of UO2 dissolution. MRS Proceedings 1518, 133

Duro, L., Tamayo, A., Bruno, J., Martínez-Esparza A. (2009). Integration of the H_2 inhibition effect of UO2 matrix dissolution into radiolytic models. Proceedings of the 12th International Conference on Environmental Remediation and Radioactive Waste Management.ICEM2009-16239.October 11-15, 2009, Liverpool, UK

Ekeroth, E., Granfors, M., Schild, D. and Spahiu, K., (2020). The effect of temperature and fuel surface area on spent nuclear fuel dissolution kinetics under H_2 atmosphere. Journal of Nuclear Materials, 531, p.151981.

Ekeroth, E., & Jonsson, M. (2003). Oxidation of UO_2 by radiolytic oxidants. *Journal of Nuclear Materials*, *322*(2-3), 242-248.

Ekeroth, E., Roth, O., & Jonsson, M. (2006). The relative impact of radiolysis products in radiation induced oxidative dissolution of UO_2. Journal of Nuclear Materials, 355(1-3), 38-46.

Elliot, A. J., & Bartels, D. M. (2009). *The reaction set, rate constants and g-values for the simulation of the radiolysis of light water over the range 20 deg to 350 deg C based on information available in 2008* (No. AECL--153-127160-450-001). Atomic Energy of Canada Limited.

Eriksen, T. E., Jonsson, M., Merino, J., (2008). Modelling time resolved and long contact time dissolution studies of spent nuclear fuel in 10 mM carbonate solution-A comparison between two models and experimental data, J. Nucl. Mater. 375, pp. 331-339.

Eriksen, T. E., Shoesmith, D. W., & Jonsson, M. (2012). Radiation induced dissolution of UO_2 based nuclear fuel–A critical review of predictive modelling approaches. *Journal of Nuclear Materials*, *420*(1-3), 409-423.

Espriu-Gascon, A., Martínez-Torrents, A., Serrano-Purroy, D., Giménez, J., de Pablo, J., & Casas, I. (2020). Contribution of phases segregated from the UO_2 matrix to the release of radionuclides from spent nuclear fuel and duration of the Instant Release Fraction (IRF). *Journal of Nuclear Materials*, *532*, 152066.

Evans, C. H. (1990). Chemical properties of biochemical relevance. In *Biochemistry of the Lanthanides* (pp. 9-46). Boston, MA: Springer US.

Evins, L.Z., Bosbach, D., Duro, L., Farnan, I., Metz, V. Riba, O. (2021) Final Scientific Report. Deliverable D1.26, DisCo project (Grant Agreement 755443), Euratom Research and Training Programme on Nuclear Energy, Horizon 2020 Framework Programme, European Commission.

Evins, L.Z, Juhola, P. and Vähänen, M. (2014). REDUPP. Final report. POSIVA-WR-14-12. Posiva Oy.

Forsyth, R. (1997). The SKB spent fuel corrosion programme. An evaluation of results from the experimental programme performed in the Studsvik Hot Cell Laboratory. SKB TR 97-25 , Svensk Kärnbränslehantering AB.

Frost, D. G., Galvin, C. O. T., Cooper, M. W. D., Obbard, E. G., Burr, P. A. (2020). Thermophysical properties of urania-zirconia $(U,Zr)O_2$ mixed oxides by molecular dynamics, Journal of Nuclear Materials 528, 151876.

Galvin, C. O., Rushton, M. J. D., Cooper, M. W. D., Andersson, D. A., Burr, P. A., & Grimes, R. W. (2021). The predicted shapes of voids and Xe bubbles in UO2. *Journal of Nuclear Materials*, *543*, 152622.

García-Gómez, S., Giménez, J., Casas, I., Llorca, J., & De Pablo, J. (2023a). X-ray photoelectron spectroscopy (XPS) study of surface oxidation of UO_2 doped with Gd_2O_3 at different temperatures and atmospheres. *Applied Surface Science*, *629*, 157429.

García-Gómez, S., Giménez, J., Casas, I., Llorca, J., & De Pablo, J. (2023b). Oxidative dissolution mechanism of both undoped and Gd_2O_3-doped UO_2(s) at alkaline to hyperalkaline pH. *Dalton Transactions*, *52*(28), 9823-9830.

Giaccardi, L., Cherubini, M., Zullo, G., Pizzocri, D., Magni, A., & Luzzi, L. (2024). Towards modelling defective fuel rods in TRANSURANUS: Benchmark and assessment of gaseous and volatile radioactive fission product release. *Annals of Nuclear Energy*, *197*, 110249.

Giorgi, R., Cechet, A., Cognini, L., Magni, A., Pizzocri, D., Luzzi, L., ... & Van Uffelen, P. (2021). A Physics-Based Description of Inter-Granular Helium Behaviour in SCIANTIX for Application in Fuel Performance Codes. In *Proceedings of Top Fuel 2021* (pp. 1-11).

Glaeser, H. (2008). GRS method for uncertainty and sensitivity evaluation of code results and applications. *Science and Technology of Nuclear Installations*.

Gonzalez, J., & Ševecek, M. (2022). Modelling of fission gas release in UO_2 doped fuel using transuranus code. *Acta Polytechnica CTU Proceedings*, *37*, 24-30.

Gonzales-Robles, E., Metz, V., Wegen, D.W., Herm, M., Papaioannou, D., Bohnert, E., Gretter, R., Müller, N., Nasyrow, R., de Weerd, W., Wiss, T., Kienzler, B. 2016. Determination of fission gas release of spent nuclear fuel in puncturing test and leaching experiments under anoxic conditions, J. Nucl. Mater. 479, pp. 67-75.

Götzmann, O., & Heuvel, H. J. (1979). Einfluss von Verunreinigungen auf die Hüllinnenkorrosion von stahlumhüllten oxidischen Brennstäben. *Journal of Nuclear Materials*, *81*(1-2), 231-239.

Grambow, B., Bruno, J., Duro, L., Merino, J., Tamayo, A., Martin, C., Pepin, G., Schumacher, S., Smidt, O., Ferry, C., Jegou, C., Quiñones, J., Iglesias, E., Villagra, N.R., Nieto, J.M., Martínez-Esparza, A., Loida, A., Metz, V., Kienzler, B., Bracke, G., Pellegrini, D., Mathieu, G., Wasselin-Trupin, V., Serres, C., Wegen, D., Jonsson, M., Johnson, L., Lemmens, K., Liu, J., Spahiu, K., Ekeroth, E., Casas, I., de Pablo, J., Watson, C., Robinson, P. and Hodgkinson, D. (2010). MICADO (Model uncertainty for the mechanism of dissolution of spent fuel in nuclear waste repository). Final report.

Grambow B, Loida A, Martinez-Esparza A, Diaz-Arcoas P, De Pablo J, Paul J-L, Marx G, Glatz J-P, Lemmens K, Ollila K, Christensen H, 2000. Source term for performance assessment of spent fuel as a waste form, European Commission, Nuclear Science and Technology, EUR 19140 EN.

Gray, W. J., Strachan, D. M., & Wilson, C. N. (1991). Gap and Grain-Boundary Inventories of Cs, Tc, and Sr in Spent LWR Fuel. MRS Online Proceedings Library, 257, 353-360.

Guo, J., Lai, H., Zhou, W., & Wei, J. (2022). Fission gas behaviors and relevant phenomena in different nuclear fuels: A review of models and experiments. *Frontiers in Energy Research*, *10*, 766865.

Guo, Z., Ma, H., Peng, D., Bao, H., Sun, Z., Xin, Y., ... & Ma, F. (2025). Temperature effects on Xe bubble structure and grain boundary migration in UO_2: A molecular dynamics simulation. *Journal of Materials Research and Technology*.

Hansson, N., Jonsson, M., Ekberg, C., Spahiu, K., (2023a). Modelling radiation-induced oxidative dissolution of UO_2-based spent nuclear fuel on the basis of the hydroxyl radical mediated surface mechanism: exploring the impact of surface reaction mechanism and spatial and temporal resolution. J. Nucl. Mater. 578, 154369.

Hansson, N. L., & Jonsson, M. (2023b). Exploring H_2-effects on radiation-induced oxidative dissolution of UO2-based spent nuclear fuel using numerical simulations. *Radiation Physics and Chemistry*, *210*, 111055.

He, H., Keech, P. G., Broczkowski, M. E., Noël, J. J., & Shoesmith, D. W. (2007). Characterization of the influence of fission product doping on the anodic reactivity of uranium dioxide. *Canadian Journal of Chemistry*, *85*(10), 702-713.

Hossain, M. M., Ekeroth, E., & Jonsson, M. (2006). Effects of HCO_3^- on the kinetics of UO_2 oxidation by H_2O_2. *Journal of nuclear materials*, *358*(2-3), 202-208.

Hummel, W. & Thoenen, T. (2023): The PSI chemical thermodynamic database 2020. Nagra Technical Report NTB 21-03.

IAEA (2010). Advanced Fuel Pellet Materials and Fuel Rod Design for Water Cooled Re-actors, International Atomic Energy Agency, Vienna.

Iglesias, L., Kokinda, J., Serrano-Purroy, D., Martínez-Torrents, A., Casas, I., de Pablo, J., ... & Giménez, J. (2023). Dissolution of high burn-up spent nuclear fuel at high-pH. *Radiochimica Acta*, *111*(11), 817-828.

Ikeuchi, H., Ishihara, M., Yano, K., Kaji, N., Nakajima, Y., & Washiya, T. (2014). Dissolution behavior of (U, Zr) O2-based simulated fuel debris in nitric acid. *Journal of Nuclear Science and Technology*, *51*(7-8), 996-1005.

Jerden Jr, J. L., Frey, K., & Ebert, W. (2015). A multiphase interfacial model for the dissolution of spent nuclear fuel. *Journal of Nuclear Materials*, *462*, 135-146.

Jegou, C., Caraballo, R., De Bonfils, J., Broudic, V., Peuget, S., Vercouter, T., Roudil, D. (2010). Oxidizing dissolution of spent MOX47 fuel subjected to water radiolysis: Solution chemistry and surface characterisation by Raman spectroscopy, J. Nucl. Mater. 399, pp. 68-80.

Jegou, C., Odorowski, M., Kerleguer, V., Broudic, V., Schlegel, M. L., Jouan, G., ... & De Windt, L. (2022). MOX Fuel corrosion processes under waste disposal conditions. *Corrosion Science*, *195*, 109964.

Johnson L.H., Garisto N. & Stroes-Gascoyne S.(1985) Used-Fuel Dissolution Studies in Canada, Proc. Waste Management, Tucson, Arizona, March 24–28, 1985, p. 479 (1985).

Johnson, L., Günther-Leopold, I., Kobler Waldis, J., Linder, H.P., Low, J., Cui, D., Ekeroth, E., Spahiu, K., Evins, L.Z., (2012). Rapid aqueous release of fission products from high burn - up LWR fuel: Experimental results and correlations with fission gas release. J. Nucl. Mater. 420, 54–62.

Jonsson M., (2023). Assessment of heterogeneous processes and parameters to be used in models for radiation induced dissolution of spent nuclear fuel, R-23-12. Svensk Kärnbränslehantering AB

Jonsson M, Nielsen F, Roth O, Ekeroth E, Nilsson S, Hossain M M, (2007). Radiation induced spent nuclear fuel dissolution under deep repository conditions. Environ. Sci. & Technol., 41, pp 7087–7093.

Johnson L., Poinssot C., Ferry C. and Lovera P. (2004). Estimates of the instant release fraction for UO2 and MOX fuel at t=0, in: A Report of the Spent Fuel Stability (SFS) Project of the 5th Euratom Framework Program, NAGRA Technical Report 04-08, Wettingen, Switzerland.

Johnson L., Ferry C., Poinssot C. and Lovera P. (2005). Spent fuel radionuclide source-term model for assessing spent fuel performance in geological disposal. Part I: Assessment of the instant release fraction. Journal of Nuclear Materials, 346, 56-65.

Johnson, L., Günther-Leopold, I., Kobler Waldis, J., Linder, H. P., Low, J., Cui, D., Ekeroth, E., Spahiu, K., & Evins, L. Z. (2012). Rapid aqueous release of fission products from high burn-up LWR fuel: Experimental results and correlations with fission gas release. *Journal of Nuclear Materials*, *420*(1–3), 54–62

Johnson L. H and McGinnes D. F. (2002). Partitioning of radionuclides in Swiss power reactor fuels. Nagra Technical Report NTB 02-07.

Johnson L. H. and Tait J. C. (1997). Release of segregated nuclides from spent fuel. SKB Technical Report TR-97-18.

Joseph, J. M., Choi, B. S., Yakabuskie, P., & Wren, J. C. (2008). A combined experimental and model analysis on the effect of pH and O_2(aq) on γ-radiolytically produced H_2 and H_2O_2. *Radiation Physics and Chemistry*, *77*(9), 1009-1020.

Kamimura K. (1992). In: Proceedings of the Technical Committee Meeting on Fission Gas Release and Fuel Rod Chemistry Related to Extended Burnup, Pembroke, Ont., Canada, 28 April–1 May 1992, IAEA-TECDOC-697, 1992, p. 82.

Kegler P, Klinkenberg M, Bukaemskiy, A., Deissmann, G., Alekseev, E.V., Bosbach, D. (2019). Chromium doped UO_2-based model systems: Synthesis and characterization of model materials for the study of the matrix corrosion of spent modern nuclear fuels. In: (Eds) Evins LZ, Valls A, Duro L, DisCo - 2 nd Annual Meeting Proceedings . Deliverable D1.15, , DisCo project (Grant Agreement 755443), Euratom Research and Training Programme on Nuclear Energy, Horizon 2020 Framework Programme, European Commission p41-48.

Kegler P, Klinkenberg M, Bukaemskiy, A., Brandt F, Deissmann, G., Bosbach, D, (2020). Chromium doped UO2-based model systems: Synthesis and characterization of model materials for the study of the matrix corrosion of spent modern nuclear fuels. In: (Eds) Evins LZ, Valls A, Duro L, DisCo – 3rd Annual Meeting Proceedings . Deliverable D1.20, DisCo project (Grant Agreement 755443), Euratom Research and Training Programme on Nuclear Energy, Horizon 2020 Framework Programme, European Commission p 44-53.

Kelm, M., Bohnert, E. (2004) A kinetic model for the radiolysis of chloride brine, its sensitivity against model parameters and a comparison with experiments, Forschungszentreum Karlsruhe, FZKA 6977.

Kerleguer, V., Jegou, C., De Windt, L., Broudic, V., Jouan, G., Miro, S., ... & Martin, C. (2020). The mechanisms of alteration of a homogeneous U0.73Pu0.27O2 MOx fuel under alpha radiolysis of water. *Journal of Nuclear Materials*, *529*, 151920.

Kienzler, B., Metz, V., Valls, A., (2014). Fast / Instant Release of Safety Relevant Radionuclides from Spent Nuclear Fuel - FIRST-Nuclides. Final scientific report Deliverable No: 5.13, Grant Agreement 295722.

Kim, J.-G., Ha, Y.-K., Park, S.-D., Jee, K.-Y., Kim, W.-H. (2001) Effect of a trivalent dopant, Gd3+, on the oxidation of uranium dioxide. Journal of Nuclear Materials, Vol. 297, pp. 327-331.

King, F., & Kolar, M. (1999). *Mathematical implementation of the mixed-potential model of fuel dissolution: model version MPM-V1. 0*. Ontario Hydro.

King, F., & Kolar, M. (2002). *Validation of the mixed-potential model for used fuel dissolution against experimental data*. Ontario Hydro, Nuclear Waste Management Division Report No. 06819-REP-01200-10077-R00.

King, F., & Kolar, M. (2003). The Mixed-Potential Model for UO2 Dissolution MPM Versions V1. 3 and V1. 4. *Ontario Hydro, Nuclear Waste Management Division Report*, (06819-REP), 01200-10104.

Kirishima, A., Akiyama, D., Kumagai, Y., Kusaka, R., Nakada, M., Watanabe, M., ... & Sato, N. (2022). Structure, stability, and actinide leaching of simulated nuclear fuel debris synthesized from UO_2, Zr, and stainless-steel. *Journal of Nuclear Materials*, *567*, 153842.

Kirkegaard, P., Bjergbakke, E. (2002). CHEMSIMUL: a simulator for chemical kinetics. Roskilde, Denmark: Riso National Laboratory, Riso-R-1085(EN).

Kleykamp, H., Paschoal, J. O., Pejsa, R., & Thümmler, F. (1985). Composition and structure of fission product precipitates in irradiated oxide fuels: Correlation with phase studies in the Mo-Ru-Rh-Pd and BaO-UO2-ZrO_2-MoO_2 Systems. Journal of Nuclear Materials, 130, 426-433.

König T., Herm M., Metz V., Rodriguez Villagra N., Elorrieta J. M., Milena-Pérez A., Bonales L. J., Gutiérrez L., Fernández-Carretero S., Núñez A., Galán H., Király M., Bertsch J., Duarte L. I., Goutam K., Schneider C., Zencker U. (2024). Final version as of 10.05.2024 of deliverable D8.10 of the HORIZON 2020 project EURAD. EC Grant agreement no: 847593.

Nilsson, S., Jonsson, M., (2008a). On the catalytic effects of UO_2(s) and Pd (s) on the reaction between H2O2 and H2 in aqueous solution. J. Nucl. Mater. 372, 160–163.

Nilsson, S., Jonsson, M., (2008b). On the catalytic effect of Pd(s) on the reduction of UO_2^{2+} with H_2 in aqueous solution. J. Nucl. Mater. 374, 290–292.

Lassmann K., Schubert A., van der Laar J. and Walker C. T. (2000). In: Fission gas behaviour in water reactor fuels. Seminar Proceedings, Cadarache, France 26-29 September 2000. Nuclear Energy Agency (NEA).

Lee, J., Kim, J., Youn, Y.-S., Liu, N., Kim, J.-G., Ha, Y.-K. *et al*. (2017) Raman study on structure of $U_{1-y}Gd_yO_{2-x}$ (y=0.005, 0.01, 0.03, 0.05 and 0.1) solid solutions, Journal of Nuclear Materials 486, 216-221.

Lemmens, K., González-Robles, E., Kienzler, B., Curti, E., Serrano-Purroy, D., Sureda, R., Martinez-Torrents, A., Roth, O., Slonski, E., Mennecart, T., Günther-Leopold, I., and Hózer, Z. (2017). Instant release of fission products in leaching experiments with high burn-up nuclear fuels in the framework of the Euratom project FIRST-Nuclides. *Journal of Nuclear Materials*, *484*, 307-323.

Li Y., Hu S., Montgomery R., Gao F. and Sun X. (2012a). Mesoscale Benchmark Demonstration Problem 1: Mesoscale Simulations of Intragranular Fission Gas Bubbles in UO_2 under Post irradiation Thermal Annealing. Report for the U. S. Department of Energy (DoE), PNNL-21295, FCR&D-MDSM-2012-000098.

Li Y., Hu S., Montgomery R., Gao F. and Sun X. (2012b). Enhanced Generic Phase-field Model of Irradiation Materials: Fission Gas Bubble Growth Kinetics in Polycrystalline UO_2. Report for the U. S. Department of Energy (DoE), PNNL-21417, FCRD-NEAMS-2012-000134.

Li, J., Liu, X., & Jonsson, M. (2023). Exploring the Change in Redox Reactivity of UO_2 Induced by Exposure to Oxidants in HCO_3^- Solution. *Inorganic Chemistry*, *62*(19), 7413-7423.

Liu X-Y, Andersson D. A. (2015). Molecular dynamics study of fission gas bubble nucleation in UO_2. J Nucl. Mater., 462:8–14.

Liu, M., Kang, Q., & Xu, H. (2020). Modelling uranium dioxide corrosion under repository conditions: A pore-scale study of the chemical and thermal processes. *Corrosion Science*, *167*, 108530.

Liu, M., Kang, Q., & Xu, H. (2021). Grain-scale study of the grain boundary effect on UO2 fuel oxidation and fission gas release under reactor conditions. *Chemical Engineering Science*, *229*, 116026.

Liu, M., Kang, Q., Xu, H., & White, J. (2023). 3D Thermal-Chemical Reactive Transport Modeling of Fluid-UO_2 Reactions under Geological Repository Conditions. *Journal of Energy Engineering*, *149*(2), 04022061.

Liu, N., Kim, J., Lee, J., Youn, Y.S., Kim, J.G., Kim, J.Y., Noël, J.J. and Shoesmith, D.W. (2017). Influence of Gd doping on the structure and electrochemical behavior of UO_2. Electrochimica Acta, 247, pp.496-504.

Liu, N., Qin, Z., Noël, J. J., & Shoesmith, D. W. (2017). Modelling the radiolytic corrosion of α-doped UO2 and spent nuclear fuel. *Journal of Nuclear Materials*, *494*, 87-94.

Liu, N., Wu, L., Qin, Z., & Shoesmith, D. W. (2016). Roles of radiolytic and externally generated H_2 in the corrosion of fractured spent nuclear fuel. *Environmental science & technology*, *50*(22), 12348-12355.

Loida, A., Gens, R., Bube, C., Lemmens, K., Cachoir, C., Mennecart, T., & Kienzler, B. (2012). Corrosion behavior of spent nuclear fuel in high pH solutions–Effect of hydrogen. MRS Online Proceedings Library (OPL), 1475, imrc11-1475.

Lösönen, P. (2000). On the behaviour of intragranular fission gas in UO2 fuel. *Journal of nuclear materials*, *280*(1), 56-72.

Lucuta, P. G., Verrall, R. A., & Palmer, B. J. (1991). Microstructural features of SIMFUEL—Simulated high-burnup UO2-based nuclear fuel. Journal of Nuclear Materials, 178(1), 48-60.

Lunev, A. V., Starikov, S. V., Aliev, T. N., & Tseplyaev, V. I. (2018). Understanding thermally-activated glide of 1/2< 110>{110} screw dislocations in UO_2–a molecular dynamics analysis. *International Journal of Plasticity*, *110*, 294-305.

Lundström T. (2003). Radiation chemistry of aqueous solutions related to nuclear reactor systems and spent fuel management, PhD-thesis, Linköping University, Dissertation No. 840.

MacInnes, D. A., & Brearley, I. R. (1982). A model for the release of fission gas from reactor fuel undergoing transient heating. *Journal of Nuclear Materials*, *107*(2-3), 123-132.

Magni, A., Di Gennaro, M., Pizzocri, D., Zullo, G., Luzzi, L., Lainet, M., ... & Van Uffelen, P. (2023). Description of new meso-scale models and their implementation in fuel performance codes. Deliverable 5.2. Partitioning And Transmuter Research Initiative in a Collaborative Innovation Action. Grant Agreement Number 945077.

Maier, A.C., Kegler, P., Klinkenberg, M., Baena, A., Finkeldei, S., Brandt, F. and Jonsson, M., (2020). On the change in UO2 redox reactivity as a function of H_2O_2 exposure. Dalton Transactions, 49(4), pp.1241-1248

MATLAB Release 2013b, MathWorks, Inc., Natick, MA, 2013

Massih, A. R. (2018). UO_2 fuel oxidation and fission gas release. *Swedish Radiation Safety Authority report, Report*, (2018), 25.

McEachern, R. J., Doern, D. C., & Wood, D. D. (1998). The effect of rare-earth fission products on the rate of U3O8 formation on UO2. *Journal of nuclear materials*, *252*(1-2), 145-149.

Mennecart, T., Lemmens K. & Cachoir C. (2014) Characterization and leaching tests for the experimental determination of IRF radionuclides from Belgian High-Burnup spent nuclear fuel. In Kinezler, B. *et al.* , Final (3rd) Annual Workshop Proceedings, FIRST-Nuclides Deliverable D5.4, Grant Agreement 295722.

Mennecart, T., Cachoir, C., Lemmens, K., Gaggiano, R., Meert, K. and Vandoorne, T., (2024). Fission product release from spent nuclear UOX fuel dissolution: Comparison between anoxic and reducing conditions and impact of pH. MRS Advances, pp.1-5.

Merino, J., Cera, E., Bruno, J., Quinones, J., Casas, I., Clarens, F., ... & Martínez-Esparza, A. (2005). Radiolytic modelling of spent fuel oxidative dissolution mechanism. Calibration against UO_2 dynamic leaching experiments. Journal of nuclear materials, 346(1), 40-47.

Metz V, 2021. Spent nuclear fuel experiments: Final results of dissolution experiments Deliverable D3.3, DisCo project (Grant Agreement 755443), Euratom Research and Training Programme on Nuclear Energy, Horizon 2020 Framework Programme, European Commission.

Michel, B., Welland, M., Ofori-Opoku, N., Vanbrutzel, L., Kulacsy, K., Tonks, M. R., ... & Crocombette, J. P. (2022). State of the art of fuel micro-mechanical modelling: From atomic scale to engineering laws in fuel performance codes. *Journal of Nuclear Materials*, *572*, 154034.

Middleburgh, S. C., Lee, W. E., & Rushton, M. J. (2021). Structure and properties of amorphous uranium dioxide. Acta Materialia, 202, 366-375.

Milena-Pérez, A., Bonales, L. J., Emblico, L., Serrano-Purroy, D., & Rodríguez-Villagra, N. (2024). Spent nuclear fuel oxidation under dry storage controlled conditions for studying its radial oxidation behavior. *Journal of Nuclear Materials*, *589*, 154831.

Milena-Pérez, A., Bonales, L.J., Rodríguez-Villagra, N., Cobos J., Galán, H. (2025) Raman spectroscopy study of the influence of additives (Cr-, Cr/Al-, and Gd) on UO_2 dissolution behavior. MRS Advances (2025). https://doi.org/10.1557/s43580-025-01172-4

Moore E, René Corrales L, Desai T, Devanathan R. (2011) Molecular dynamics simulation of Xe bubble nucleation in nanocrystalline UO2 nuclear fuel. J Nucl Mater., 419:140–4.

Muzeau, B., Jégou, C., Delaunay, F., Broudic, V., Brevet, A., Catalette, H., ... & Corbel, C. (2009). Radiolytic oxidation of UO_2 pellets doped with alpha-emitters (238/239Pu). *Journal of Alloys and Compounds*, *467*(1-2), 578-589.

Nardi, A., Idiart, A., Trinchero, P., de Vries, L. M., and J. Molinero (2014). Interface COMSOL-PHREEQC (iCP), an efficient numerical framework for the solution of coupled multiphysics and geochemistry. Computers & Geosciences 69: 10-21.

Neck, V. and Kim, J.I., 2001. Solubility and hydrolysis of tetravalent actinides. Radiochimica Acta, 89(1), pp.1-16.

Nogita, K., & Une, K. (1997). Formation of pellet-cladding bonding layer in high burnup BWR fuels. Journal of nuclear science and technology, 34(7), 679-686.

Odorowski, M., Jegou, C., De Windt, L., Broudic, V., Jouan, G., Peuget, S., & Martin, C. (2017). Effect of metallic iron on the oxidative dissolution of UO2 doped with a radioactive alpha emitter in synthetic Callovian-Oxfordian groundwater. *Geochimica et cosmochimica acta*, *219*, 1-21.

Odorowski, M., Jegou, C., de Windt, L., Broudic, V., Peuget, S., Magnin, M., Tribet, M., Martin, C. (2016). Oxidative dissolution of unirradiated Mimas MOX fuel (U/Pu oxide) in carbonated water under oxic and anoxic conditions. J. Nucl. Mater. 468 p. 17-25.

Olander, D. R. (1976). *Fundamental aspects of nuclear reactor fuel elements: solutions to problems* (No. TID-26711-P2). California Univ., Berkeley (USA). Dept. of Nuclear Engineering.

Olander, D. R., & Van Uffelen, P. (2001). On the role of grain boundary diffusion in fission gas release. *Journal of nuclear materials*, *288*(2-3), 137-147.

Olander, D. R., & Wongsawaeng, D. (2006). Re-solution of fission gas–A review: Part I. Intragranular bubbles. *Journal of nuclear materials*, *354*(1-3), 94-109.

Olds, T. A., Karcher, S. E., Kriegsman, K. W., Guo, X., & McCloy, J. S. (2020). Oxidation and anion lattice defect signatures of hypostoichiometric lanthanide-doped UO_2. *Journal of Nuclear Materials*, *530*, 151959.

Ollila, K., Albinsson, Y., Oversby, V., & Cowper, M. (2003). Dissolution rates of unirradiated UO_2, UO_2 doped with 233U, and spent fuel under normal atmospheric conditions and under reducing conditions using an isotope dilution method (No. SKB-TR--03-13). Swedish Nuclear Fuel and Waste Management Co.

Ollila, K., Myllykylä, E., Tanhua-Tyrkkö, M., & Lavonen, T. (2013). Dissolution rate of alpha-doped UO2 in natural groundwater. *Journal of nuclear materials*, *442*(1-3), 320-325.

Ollila, K., & Oversby, V. M. (2005). Dissolution of unirradiated UO_2 and UO_2 doped with 233U under reducing conditions (No. SKB-TR--05-07). Swedish Nuclear Fuel and Waste Management Co..

Ollila, K. (2006*).* Dissolution of unirradiated UO2 and UO2 doped with 233U in 0.01 M NaCl under anoxic and reducing conditions (No. POSIVA--06-08). Posiva Oy.

Park, K., Olander, D.R. (1992) Defect models for the oxygen potentials of gadolinium-and europium-doped urania. Journal of Nuclear Materials, Vol. 187, pp. 89-96.

Parras, J. P., & De Souza, R. A. (2020). Grain-boundary diffusion of cations in fluorite-type oxides is faster but not always easier. Acta Materialia, 195, 383-391.

Parrish, R., & Aitkaliyeva, A. (2018). A review of microstructural features in fast reactor mixed oxide fuels. Journal of nuclear materials, 510, 644-660.

Pastore, G., Barani, T., Pizzocri, D., Magni, A., & Luzzi, L. (2018). Modeling fission gas release and bubble evolution in UO2 for engineering fuel rod analysis. *in: TopFuel2018 - Reactor Fuel Performance, 30 September - 04 October 2018, Prague, Czech Republic.*

Pastore G., Luzzi L,. Di Marcello V. and Van Uffelen P. (2013). Physics-based modelling of fission gas swelling and release in UO_2 applied to integral fuel rod analysis. Nuclear Enginering and Design, 256, 75-86.

Pastore, G., Swiler, L. P., Hales, J. D., Novascone, S. R., Perez, D. M., Spencer, B. W., ... & Williamson, R. L. (2015). Uncertainty and sensitivity analysis of fission gas behavior in engineering-scale fuel modeling. *Journal of Nuclear Materials*, *456*, 398-408.

Pehrman, R., Trummer, M., Lousada, C. M., & Jonsson, M. (2012). On the redox reactivity of doped UO2 pellets–Influence of dopants on the H_2O_2 decomposition mechanism. Journal of Nuclear Materials, 430(1-3), 6-11.

Pękala, M., Idiart, A., Duro, L., & Riba, O. (2013). DELIVERABLE 4.2. Models for fission products release from nuclear fuel and their applicability to the FIRST-NUCLIDES project. In *2nd Annual Workshop Proceedings of the Collaborative Project "Fast/Instant Release of Safety Relevant Radionuclides from Spent Nuclear Fuel"* (p. 61).

Poinssot, C., Ferry, C., Kelm, M., Cavedon, J. M., Corbel, C., Jegou, C., ... & Pablo, J. D. (2005). *Spent fuel stability under repository conditions-final report of the European Project* (No. CEA-R--6093). CEA Saclay.

Puranen, A., Granfors, M., Ekeroth, E., & Spahiu, K. (2016). Lessons learned from leaching of dry milled high burnup UO_2 fuel under H_2 atmosphere. MRS Advances, 1(62), 4169-4175.

Puranen, A., Roth, O., Evins, L. Z., & Spahiu, K. (2018). Aqueous leaching of high burnup UO_2 fuel under hydrogen conditions. MRS Advances, 3(19), 1013-1018.

Puranen, A., Barreiro, A., Evins, L. Z., & Spahiu, K. (2020). Spent fuel corrosion and the impact of iron corrosion–The effects of hydrogen generation and formation of iron corrosion products. Journal of Nuclear Materials, 542, 152423.

Puranen, A., Evins, L. Z., Barreiro, A., Roth, O., & Spahiu, K. (2022). Very high burnup spent fuel corrosion & leaching under hydrogen conditions. Journal of Nuclear Materials, 572, 154027.

Razdan, M., & Shoesmith, D. W. (2013). Influence of trivalent-dopants on the structural and electrochemical properties of uranium dioxide (UO_2). *Journal of The Electrochemical Society*, *161*(3), H105.

Rest, J. (2003). The effect of irradiation-induced gas-atom re-solution on grain-boundary bubble growth. *Journal of nuclear materials*, *321*(2-3), 305-312.

Rest, J., Cooper, M. W., Spino, J., Turnbull, J. A., Van Uffelen, P., & Walker, C. T. (2018). Fission gas release from UO2 nuclear fuel: A review. *Journal of Nuclear Materials*, *513*, 310-345.

Rest J. and Zawadzki S. A. (1992). FASTGRASS: A Mechanistic Model for the Prediction of Xe, I, Cs, Te, Ba, and Sr Release from Nuclear Fuel under Normal and Severe-Accident Conditions. User's Guide for Mainframe, Workstation, and Personal Computer Applications. Argonne National Laboratory (ANL), NUREG/CR-584O, ANL- 92/3.

Riba, O., Coene, E., Silva, O., Duro, L. (2020). Spent fuel alteration model integrating processes of different time-scales. MRS Advances, 5(3), 159-166.

Riba, O., Coene, E., Silva, O., Duro, L. (2021). Development of a reactive transport model of spent fuel dissolution under near field environmental conditions. Deliverable 5.5, DisCo project (Grant Agreement 755443), Euratom Research and Training Programme on Nuclear Energy, Horizon 2020 Framework Programme, European Commission.

Rodríguez-Villagra, N., Bonales, L. J., Fernández-Carretero, S., Milena-Pérez, A., Gutierrez, L., & Galán, H. (2023). Exploring a surrogate of Pellet–Cladding interaction: Characterization and oxidation behavior. *MRS Advances*, *8*(6), 238-242.

Rodríguez-Villagra, N., Fernández, S., Jiménez-Bonales, L., Milena-Pérez, A., Núñez, A., Durán, S., ... & Cobos, J. (2020). Production of unirradiated advanced doped UO_2 fuel for dissolution studies at repository conditions. In *3 rd Annual Meeting Proceedings* (p. 79).

Rodríguez-Villagra, N., Fernández-Carretero, S., Milena-Pérez, A., Bonales, L. J., Gutierrez, L., Cobos, J., & Galán, H. (2025). Impact of dopants and leachants on modern UO_2-based fuels alteration under final storage conditions: single and joint effects. *Journal of Nuclear Materials*, 155635.

Rodríguez-Villagra, N., Riba, O., Milena-Pérez, A., Cobos, J., Jimenez-Bonales, L., Fernández-Carretero, S., ... & Duro, L. (2022). Dopant effect on the spent fuel matrix dissolution of new advanced fuels: Cr-doped UO2 and Cr/Al-doped UO_2. *Journal of Nuclear Materials*, *568*, 153880.

Rondinella, V. V., Cobos, J., & Wiss, T. (2004). Leaching Behaviour of Low-Activity Alpha-Doped UO2. *MRS Online Proceedings Library (OPL)*, *824*, CC9-8.

Rondinella, V. V., & Wiss, T. (2010). The high burn-up structure in nuclear fuel. Materials today, 13(12), 24-32.

Roth, O., Cui, D., Askeljung, C., Puranen, A., Evins, L.Z., Spahiu, K. 2019. Leaching of spent nuclear fuels in aerated conditions: Influences of sample preparation on radionuclide release patterns, J. Nucl. Mater. 527, paper 151789.

Roth, O., Jonsson M., (2008). Oxidation of UO_2(s) in aqueous solutions, Centr. Eur. J. Chem. 6, pp. 1-14.

Römer, J., Plaschke, M., Beuchle, G., & Kim, J. I. (2003). In situ investigation of U (IV)-oxide surface dissolution and remineralization by electrochemical AFM. Journal of nuclear materials, 322(1), 80-86.

Sasaki, T., Takeno, Y., Kirishima, A., & Sato, N. (2014). Leaching test of gamma-emitting Cs, Ru, Zr, and U from neutron-irradiated UO_2/ZrO_2 solid solutions in non-filtered surface seawater: Fukushima NPP Accident Related. *Journal of Nuclear Science and Technology*, *52*(2), 147-151.

Scheele, R. D., Hanson, B. D., Casella, A. M. (2021). Effect of added gadolinium oxide on the thermal air oxidation of uranium dioxide, Journal of Nuclear Materials 552, 153008

Scheele, R. D., Hanson, B. D., Cumblidge, S. E., Jenson, E. D., Kozelisky, A. E., Sell, R. L., ... & Snow, L. A. (2004). Effect of Gadolinium Doping on the Air Oxidation of Uranium Dioxide. *MRS Online Proceedings Library (OPL)*, *824*, CC8-8.

Shoesmith, D. W., Kolar, M., & King, F. (2003). A mixed-potential model to predict fuel (uranium dioxide) corrosion within a failed nuclear waste container. *Corrosion*, *59*(9), 802-816.

SKB 2022, Post-closure safety for the final repository for spent nuclear fuel at Forsmark. Data report, PSAR version, TR-21-06. Svensk Kärnbränslehantering AB.

Smith, H., Cordara, T., Mohun, R., Stennett, M.C., Hyatt, N.C. and Corkhill, C.L (2020). Assessment of long-term durability of Cr_2O_3 doped UO_2. In Evins *et al.*. (Eds) 3rd Annual Meeting Proceedings. Deliverable D1.20 , DisCo project (Grant Agreement 755443), Euratom Research and Training Programme on Nuclear Energy, Horizon 2020 Framework Programme, European Commission, p. 89-94.

Smith, H., Townsend, L. T., Mohun, R., Cordara, T., Stennett, M. C., Mosselmans, J. F. W., ,Kvashnina K., & Corkhill, C. L. (2022). Cr^{2+} solid solution in UO_2 evidenced by advanced spectroscopy. Communications Chemistry, 5(1), 163.

Smith, H., Cordara, T., Gausse, C., Pepper, S. E., & Corkhill, C. L. (2023). Oxidative dissolution of Cr-doped UO_2 nuclear fuel. npj Materials Degradation, 7(1), 25.

Spahiu, K. (2021). Spent Nuclear Fuel Domain 3.1. *EURAD State of Knowledge Report, Version*, *1*.

Spahiu K., and Evins, L.Z. (2013). Metal alloy particles in spent nuclear fuel. SKBdoc 1415408 ver. 1.0 Svensk Kärnbränslehantering AB.

Speight, M. V., & Turnbull, J. A. (1977). Enhanced fission-product release by grain-boundary diffusion. Journal of Nuclear Materials, 68(2), 244-249.

Spino, J. (1998). State of the technology review. In Advances in Fuel Pellet Technology for Improved Performance at High Burnup. IAEA-TECDOC-1036, Proc. of a Technical Committee Meeting, Tokyo, 28 October - 1 November 1996. IAEA, Vienna.

Tarasov V. I. and Veshchunov M. S. (2009). An advanced model for grain face diffusion transport in irradiated UO_2 fuel. Part 2: Model implementation and validation. Journal of Nuclear Materials 392, 85-8.

Thomas, L. E., Beyer, C. E., & Chariot, L. A. (1992). Microstructural analysis of LWR spent fuels at high burnup. Journal of Nuclear Materials, 188, 80-89.

Tonna, R., Sasaki, T., Kodama, Y., Kobayashi, T., Akiyama, D., Kirishima, A., ... & Watanabe, M. (2023). Phase analysis of simulated nuclear fuel debris synthesized using UO_2, Zr, and stainless steel and leaching behavior of the fission products and matrix elements. *Nuclear Engineering and Technology*, *55*(4), 1300-1309.

Tonna, R., Sasaki, T., Okamoto, Y., & Kobayashi, T. (2023). Interpretation of Dissolution Behavior at the Surface of Uranium-Zirconium Oxide Solid Solutions. *Available at SSRN 5023286*.

Tonks, M., Andersson, D., Devanathan, R., Dubourg, R., El-Azab, A., Freyss, M., ... & Welland, M. (2018). Unit mechanisms of fission gas release: Current understanding and future needs. *Journal of Nuclear Materials*, *504*, 300-317.

Trummer, M., Nilsson, S., Jonsson, M. (2008). On the effects of fission product noble metal inclusions on the kinetics of radiation induced dissolution of spent nuclear fuel, J. Nucl. Mater. 378, pp. 55-59.

Turnbull, J. A. (1974). The effect of grain size on the swelling and gas release properties of UO2 during irradiation. *Journal of Nuclear Materials*, *50*(1), 62-68.

Turnbull, J. A., & Tucker, M. O. (1974). Swelling in UO2 under conditions of gas release. *Philosophical Magazine*, *30*(1), 47-63.

Turnbull, J. A., & Friskney, C. A. (1978). The relation between microstructure and the release of unstable fission products during high temperature irradiation of uranium dioxide. *Journal of Nuclear Materials*, *71*(2), 238-248.

Van Uffelen P. (2002). Contribution to the modelling of fission gas release in Light Water Reactor fuel. Doctoral Thesis, University of Liege.

Veshchunov, M. S. (2008). Modelling of grain face bubbles coalescence in irradiated UO_2 fuel. *Journal of Nuclear Materials*, *374*(1-2), 44-53.

Veshchunov, M. S., Boldyrev, A. V., Kuznetsov, A. V., Ozrin, V. D., Seryi, M. S., Shestak, V. E., ... & Yanilkin, A. V. (2015). Development of the advanced mechanistic fuel performance and safety code using the multi-scale approach. *Nuclear Engineering and Design*, *295*, 116-126.

Veshchunov, M.S., Boldyrev, A.V., Ozrin, V.D., Shestak, V.E., Tarasov, V.I., (2011). A New Mechanistic Code SFPR for Modeling of Single Fuel Rod Performance underVarious Regimes of LWR Operation. Nucl. Eng. Des. 241, 2822–2830.

Veshchunov, M. S., Dubourg, R., Ozrin, V. D., Shestak, V. E., & Tarasov, V. I. (2007). Mechanistic modelling of urania fuel evolution and fission product migration during irradiation and heating. *Journal of nuclear materials*, *362*(2-3), 327-335.

Veshchunov, M.S., Ozrin, V.D., Shestak, V.E., Tarasov, V.I., Dubourg, R., Nicaise, G., (2006). Development of the mechanistic code MFPR for modelling fission products release from irradiated UO_2 fuel. Nucl. Eng. Des. 236, 179–200.

Veshchunov M. S. and Shestak V. E. (2008). An advanced model for intragranular bubble diffusivity in irradiated UO_2 fuel. Journal of Nuclear Materials 376, 174-180.

Veshchunov M. S. and Tarasov V. I. (2009). An advanced model for grain face diffusion transport in irradiated UO_2 fuel. Part 1: Model formulation. Journal of Nuclear Materials 392, 78-84.

Vinograd, V. L., Bukaemskiy, A. A., Deissmann, G., & Modolo, G. (2023). Thermodynamic model of the oxidation of Ln-doped UO2. Scientific Reports, 13(1), 17944.

Vlassopoulos, E., Dagan, R., Fiorito, L., Herm, M., Jansson, P., Kromar, M., ... & Žerovnik, G. (2024). EURAD WP8: Spent Fuel Characterisation and Evolution Until Disposal. D 8.2 Updated State-of-the-Art Report.

Wang, Z., Yu, M., Yang, C., Long, X., Gao, N., Yao, Z., ... & Wang, X. (2022). Effect of Radiation Defects on Thermo–Mechanical Properties of UO_2 Investigated by Molecular Dynamics Method. *Metals*, *12*(5), 761.

White, R. J. (2004). The development of grain-face porosity in irradiated oxide fuel. *Journal of Nuclear Materials*, *325*(1), 61-77.

White, R. J., & Tucker, M. O. (1983). A new fission-gas release model. *Journal of nuclear materials*, *118*(1), 1-38.

White, R. J., & Tucker, M. O. (1994, April). A new mechanistic model for the calculation of fission gas release. In *ANS/IAEA International Topical Meeting on Light Water Reactor Fuel Performance held at West Palm Beach, Florida, USA*.

Wilks, S. S. (1942). Statistical prediction with special reference to the problem of tolerance limits. *The Annals of Mathematical Statistics*, *13*(4), 400–409.

Willett, C. D., Kimmig, S. R., Cassata, W. S., Isselhardt, B. H., Liezers, M., Eiden, G. C., & Wacker, J. F. (2020). Fission Gas Measurements in Spent Fuel: Literature Review. LLNL-TR-815309. Lawrence Livermore National Laboratory.

Wu, L., Beauregard, Y., Qin, Z., Rohani, S., & Shoesmith, D. W. (2012). A model for the influence of steel corrosion products on nuclear fuel corrosion under permanent disposal conditions. *Corrosion Science*, *61*, 83-91.

Wu, L., Liu, N., Qin, Z., Shoesmith, D.W. (2014a). Modeling the radiolytic corrosion of fractured nuclear fuel under permanent disposal conditions. Journal of The Electrochemical Society, 161(8), E3259-E3266.

Wu, L., Qin, Z., Shoesmith, D. W. (2014b). An improved model for the corrosion of used nuclear fuel inside a failed waste container under permanent disposal conditions. Corrosion Science, 84, 85-95.

Xia, Y., Wang, Z., Wang, L., Chen, Y., Liu, Z., Wang, Q., ... & Deng, H. (2022). Molecular Dynamics Simulations of Xe Behaviors at the Grain Boundary in UO_2. *Metals*, *12*(5), 763.

Xiao-Feng, T., Chong-Sheng, L., Zheng-He, Z., & Tao, G. (2010). Molecular dynamics simulation of collective behaviour of Xe in UO_2. *Chinese Physics B*, *19*(5), 057102.

Zwicky H-U, Low J, Ekeroth E, 2011. Corrosion studies with high burnup light water reactor fuel. Release of nuclides into simulated groundwater during accumulated contact time of up to two years. TR-11-03 Svensk Kärnbränslehantering AB.